2005a). Regarding the involvement of BCRP in biliary excretion, some reports have demonstrated that the biliary excretion of 2-amino-1-methyl-6-phenylimidazo(4,5-*b*)pyridine and nitrofurantoin is almost impaired in Bcrp1(−/−) mice (van Herwaarden et al., 2003; Merino et al., 2005a) and that the biliary excretion of topotecan and cimetidine is also mainly regulated by Bcrp, considering the gender difference in the hepatic expression level of Bcrp and the plasma concentration profiles (Merino et al., 2005b). In addition, it has been demonstrated that certain kinds of single-nucleotide polymorphisms (SNPs) in BCRP and inhibition of BCRP-mediated transport by some compounds may alter its function and the pharmacokinetics of some drugs in vitro (Imai et al., 2002; Zamber et al., 2003; Kondo et al., 2004) as well as in vivo (Kruijtzer et al., 2002; Sparreboom et al., 2004). Therefore, the pharmacokinetics of several important compounds are regulated mainly by BCRP.

Pitavastatin is a highly potent inhibitor of 3-hydroxymethylglutaryl coenzyme A (HMG-CoA) reductase, the rate-limiting enzyme in cholesterol biosynthesis (Kajinami et al., 2003). Pitavastatin causes a significant reduction in not only serum total cholesterol and low-density lipoprotein cholesterol but also triglyceride levels (Stein et al., 1998). It has been demonstrated that [^{14}C]pitavastatin is distributed selectively to the liver in rats with a liver-to-plasma concentration ratio of more than 50 (Kimata et al., 1998). We demonstrated previously that pitavastatin is taken up into human hepatocytes mainly by OATP1B1 (OATP2/OATP-C) (Hirano et al., 2004). Then, because it is scarcely metabolized in human liver microsomes (Fujino et al., 2003), pitavastatin is supposed to be excreted into bile in unchanged form (Kojima et al., 2001). However, the biliary transport mechanism of pitavastatin has not been clarified yet. So far, Fujino et al. (2002) have demonstrated that after intravenous bolus administration of pitavastatin, its plasma concentration and biliary excretion in Eisai hyperbilirubinemic rats (EHBRs), an Mrp2-deficient rat, are comparable with those in Sprague-Dawley rats and that the plasma and brain concentrations of pitavastatin in mdr1a/1b knockout mice are not different from those in control mice. In addition, we have already shown that pitavastatin is not a substrate of rat and human BSEP (Hirano et al., 2005). These results suggest that BSEP, MRP2, and MDR1 do not make a major contribution to the biliary excretion of pitavastatin.

In the present study, to demonstrate the involvement of BCRP in the biliary excretion of pitavastatin, we examined the transport of pitavastatin by transporter expression systems and observed the biliary excretion clearance of pitavastatin in transporter-deficient animals. Moreover, to check whether other statins could be substrates of BCRP or not, we performed a transport study using BCRP-expressing membrane vesicles.

Materials and Methods

Animals. Male Bcrp1(−/−) and wild-type FVB mice (16–18 weeks old) were used in the present study (Jonker et al., 2002). Male Sprague-Dawley rats (7–8 weeks old) and EHBRs (7–8 weeks old) were purchased from Nippon SLC (Shizuoka, Japan). All animals were maintained under standard conditions with a reverse dark-light cycle and were treated humanely. Food and water were available ad libitum. The studies reported in this manuscript were carried out in accordance with the guidelines provided by the Institutional Animal Care Committee (Graduate School of Pharmaceutical Sciences, The University of Tokyo, Tokyo, Japan).

Materials. Pitavastatin, monocalcium bis[(3*R*,5*S*,6*E*)-7-[2-cyclopropyl-4-(4-fluorophenyl)-3-quinolyl]3,5-dihydroxy-6-hepteonate] was synthesized by Nissan Chemical Industries (Chiba, Japan). [^{3}H]Pitavastatin (16.0 Ci/mmol) and [^{3}H]cerivastatin (4.86 Ci/mmol) were synthesized by Amersham Biosciences UK, Ltd. (Little Chalfont, Buckinghamshire, UK) and Hartmann Analytic GmbH (Braunschweig, Germany), respectively. [^{3}H]Pravastatin (44.6 Ci/mmol), [^{14}C]fluvastatin (45.7 mCi/mmol), and [^{3}H]rosuvastatin (79 Ci/mmol) were supplied by Sankyo Co., Ltd. (Tokyo, Japan), Novartis Pharma K.K. (Basel, Switzerland), and AstraZeneca PLC (London, UK), respectively. Other unlabeled HMG-CoA reductase inhibitors (atorvastatin, cerivastatin, fluvastatin, pravastatin, rosuvastatin, and simvastatin acid) were donated by Kowa Co., Ltd. (Tokyo, Japan). [^{3}H]17β-Estradiol-17β-D-glucuronide ($E_2$17βG) and [^{3}H]estrone-3-sulfate (45 and 46 Ci/mmol, respectively) were purchased from PerkinElmer Life and Analytical Sciences (Boston, MA). Unlabeled $E_2$17βG and estrone-3-sulfate were purchased from Sigma-Aldrich (St. Louis, MO). All other chemicals were of analytical grade and were commercially available.

Cell Culture. Human BCRP-, mouse Bcrp-, or green fluorescent protein (GFP)-transfected HEK293 cells (Kondo et al., 2004) and MDCK II single- and double-transfected cells expressing human OATP1B1, MDR1, MRP2, or BCRP (Matsushima et al., 2005) and rat Oatp1b2 or Mrp2 (Sasaki et al., 2004) were grown in Dulbecco's modified Eagle's medium low glucose (Invitrogen, Carlsbad, CA) supplemented with 10% fetal bovine serum (Sigma-Aldrich), 100 U/ml penicillin, and 100 μg/ml streptomycin at 37°C with 5% CO_2 and at 95% humidity.

Construction and Infection of Recombinant Adenovirus and the Membrane-Vesicle Preparation. Details of the procedure for producing recombinant adenovirus containing human BCRP, mouse Bcrp, and GFP have been described previously (Kondo et al., 2004). Membrane vesicles were prepared from BCRP and GFP-transfected HEK293 cells according to the method described previously (Kondo et al., 2004). For the preparation of the isolated membrane vesicles, HEK293 cells cultured in a 15-cm dish were infected by recombinant adenovirus containing human and mouse BCRP cDNA (multiplicity of infection = 10). As a negative control, cells were infected with GFP (multiplicity of infection = 10). Cells were harvested 48 h after infection, and then the membrane vesicles were isolated from 1 to 2 × 10^8 cells using a standard method described previously in detail (Muller et al., 1994). In brief, cells were diluted 40-fold with hypotonic buffer (1 mM Tris-HCl and 0.1 mM EDTA, pH 7.4, at 37°C) and stirred gently for 1 h on ice in the presence of 2 mM phenylmethylsulfonyl fluoride, 5 μg/ml leupeptin, 1 μg/ml pepstatin, and 5 μg/ml aprotinin. The cell lysate was centrifuged at 100,000*g* for 30 min at 4°C, and the resulting pellet was suspended in 10 ml of isotonic TS buffer (10 mM Tris-HCl and 250 mM sucrose, pH 7.4 at 4°C) and homogenized using a Dounce B homogenizer (glass/glass, tight pestle, 30 strokes). The crude membrane fraction was layered on top of 38% (w/v) sucrose solution in 5 mM Tris-HEPES, pH 7.4, at 4°C, and centrifuged in Beckman SW41 rotor centrifuged at 280,000*g* for 60 min at 4°C. The turbid layer at the interface was collected, diluted to 23 ml with TS buffer, and centrifuged at 100,000*g* for 30 min at 4°C. The resulting pellet was suspended in 400 μl of TS buffer. Vesicles were formed by passing the suspension 30 times through a 27-gauge needle using a syringe. The membrane vesicles were finally frozen in liquid nitrogen and stored at −80°C until use. Protein concentrations were determined by the Lowry method, and bovine serum albumin was used as a standard.

Transport Studies with Membrane Vesicles. The transport studies were performed using a rapid filtration technique (Hirohashi et al., 1999). In brief, 15 μl of transport medium (10 mM Tris-HCl, 250 mM sucrose, and 10 mM $MgCl_2$, pH 7.4) containing radiolabeled compounds, with or without unlabeled substrate, was preincubated

at 37°C for 3 min and then rapidly mixed with 5 μl of membrane vesicle suspension (5 μg of protein). The reaction mixture contained 5 mM ATP or AMP along with the ATP-regenerating system (10 mM creatine phosphate and 100 μg/μl creatine phosphokinase). The transport reaction was terminated by the addition of 1 ml of ice-cold buffer containing 10 mM Tris-HCl, 250 mM sucrose, and 0.1 M NaCl, pH 7.4. The stopped reaction mixture was filtered through a 0.45-μm hemagglutinin filter (Millipore Corporation, Billerica, MA) and then washed twice with 5 ml of stop solution. Radioactivity retained on the filter was determined in a liquid scintillation counter (LS6000SE; Beckman Coulter, Inc., Fullerton, CA) after the addition of scintillation cocktail (Clear-sol I; Nacalai Tesque, Tokyo, Japan).

Transcellular Transport Study. Transfected MDCK II cells were seeded in 24-well plates at a density of 1.4×10^5 cells/well and were cultured with 10 mM sodium butyrate for 24 h before the transport study (Sasaki et al., 2002). Krebs-Henseleit buffer consisted of 142 mM NaCl, 23.8 mM Na_2CO_3, 4.83 mM KCl, 0.96 mM KH_2PO_4, 1.20 mM $MgSO_4$, 12.5 mM HEPES, 5 mM glucose, and 1.53 mM $CaCl_2$ adjusted to pH 7.4. The experiments were initiated by replacing the medium on either the apical or basal side of the cell layer with complete medium containing tritium-labeled and unlabeled $E_2$17βG or pitavastatin (0.1 μM). The cells were incubated at 37°C, and aliquots of medium were taken from each compartment at designated time points. Radioactivity in 100 μl of medium was measured in a liquid scintillation counter (LS6000SE; Beckman Coulter) after the addition of scintillation cocktail (Clear-sol I; Nacalai Tesque). At the end of the experiments, the cells were washed three times with 1.5 ml of ice-cold Krebs-Henseleit buffer and solubilized in 450 μl of 0.2 N NaOH. After the addition of 225 μl of 0.4 N HCl, 600-μl aliquots were transferred to scintillation vials. Aliquots (50 μl) of cell lysate were used to determine protein concentrations as described above.

Kinetic Analysis. Ligand uptake was normalized in terms of the amount of membrane protein and expressed as the uptake volume [μl/mg protein], given as the amount of radioactivity associated with the cells [dpm/mg protein] divided by its concentration in the incubation medium [dpm/μl]. The ATP-dependent uptake of ligands via BCRP was calculated by subtracting the ligand in the presence of AMP from that in the presence of ATP. Kinetic parameters were obtained using the equation $v = (V_{max} \times S)/(K_m + S)$, where v is the uptake velocity of the substrate (in picomoles per minute per milligram of protein), S is the substrate concentration in the medium (in micromolars), K_m is the Michaelis constant (in micromolars), and V_{max} is the maximum uptake velocity (in picomoles per minute per milligram of protein). The Damping Gauss Newton Method algorithm was used with a MULTI program (Yamaoka et al., 1981) to perform nonlinear least-squares data fitting. Inhibition constants (K_i) of a series of compounds were calculated with the use of the following equation (if the substrate concentration was much lower than the K_m value): $CL(+I) = CL/(1 + I/K_i)$, where CL represents the uptake clearance in the absence of inhibitor, $CL(+I)$ represents the uptake clearance in the presence of inhibitor, and I represents the concentration of the inhibitor. When fitting the data to determine the K_i value, the input data were weighed as the reciprocal of the observed values.

In Vivo Infusion Study in Rats. Male Sprague-Dawley rats and EHBRs weighing approximately 250 to 300 g were used for these experiments. Under pentobarbital anesthesia (30 mg/kg), the femoral vein was cannulated with a polyethylene catheter (PE-50) for the injection of [^{3}H]pitavastatin. The bile duct was cannulated with a polyethylene catheter (PE-10) for bile collection. The rats received a constant infusion of pitavastatin at a dose of 72 μg/h/kg after a bolus intravenous administration of 0.25 mg/kg. Blood samples were collected from the jugular vein. Bile was collected in preweighed test tubes at 30-min intervals throughout the experiment. Plasma was prepared by centrifugation of the blood samples (10,000g, Microfuge; Beckman Coulter). The rats were killed after 210 min, and the entire liver was excised immediately. Then the liver was weighed and minced, and subsequently 200 μl of hydroxyperoxide and 400 μl of isopropanol were added to approximately 200 mg of liver. This was incubated at 55°C for 4 to 6 h after the addition of 2 ml of soluene (PerkinElmer Life and Analytical Sciences) to dissolve the tissues, and then the radioactivity was determined in a liquid scintillation counter after the addition of scintillation cocktail.

In Vivo Infusion Study in Mice and Quantification of Pitavastatin by LC/MS. Male FVB and Bcrp1(−/−) mice weighing approximately 28 to 33 g were used throughout these experiments. Under pentobarbital anesthesia (30 mg/kg), the jugular vein was cannulated with a polyethylene catheter (PE-10) for the injection of pitavastatin. The bile duct was cannulated with a polyethylene catheter (SP-8) for bile collection. The mice received a constant infusion of pitavastatin at a dose of 300 μg/h/kg. Blood samples were collected from the opposite jugular vein. Bile was collected in preweighed test tubes at 15-min intervals throughout the experiments. Plasma was prepared by centrifugation of the blood samples. The mice were killed after 150 min, and the entire liver, kidney, brain, and skeletal muscle were excised immediately. The tissues were weighed and stored at −80°C until quantification. Portions of liver, kidney, brain, and skeletal muscle were added to five volumes of physiological saline (w/v) and homogenized. Plasma (10 μl), bile (1 μl), or tissue homogenate (10 or 100 μl) was deproteinized with 200 μl of methanol containing the internal standard (40 ng/ml atorvastatin), followed by centrifugation at 4°C and 10,000g for 10 min. The supernatant (100 μl) was mixed with 50 μl of water and subjected to high-performance liquid chromatography (Waters 2695; Waters, Milford, MA). The LC/MS analysis of pitavastatin was performed using an Inertsil ODS-3 column (50 × 2.1 mm; particle size, 5 μm) (GL Sciences, Tokyo, Japan). The mobile phase consisted of methanol/ammonium formate buffer, pH 4 = 7:3 (v/v), and the flow rate was 0.7 ml/min. The MS instrument used for this work was a ZQ micromass (Waters) equipped with a Z-spray source; it was operated in the positive-ion electrospray ionization mode. The Z-spray desolvation temperature, capillary voltage, and cone voltage were 350°C, 3400 V, and 40 V, respectively. The m/z monitored for pitavastatin and atorvastatin was 422.3 and 559.0, respectively. No chromatographic interference was found for pitavastatin and atorvastatin in extracts from blank plasma, bile, and tissue homogenates. The retention times of pitavastatin and atorvastatin were 1.2 and 1.1 min, respectively. The detection limits for pitavastatin were 5, 2000, 100, 5, 5, and 5 ng/ml in plasma, bile, liver, kidney, brain, and muscle, respectively.

Pharmacokinetic Analysis. Total plasma clearance (CL_{total}), biliary clearance normalized by circulating plasma ($CL_{bile,plasma}$), and biliary clearance normalized by the liver concentration ($CL_{bile,liver}$) were calculated from the equations $CL_{total} = I/C_{ss,plasma}$, $CL_{bile,plasma} = V_{bile}/C_{ss,plasma}$, and $CL_{bile,\ liver} = V_{bile}/C_{ss,liver}$, where I, $C_{ss,plasma}$, V_{bile}, and $C_{ss,liver}$ represent the infusion rate (in micrograms per minute per kilogram), plasma concentrations at steady state (in nanograms per milliliter), biliary excretion rate at steady state (in micrograms per minute per kilogram), and hepatic concentration at steady state (in nanograms per milliliter), respectively. In rats, $C_{ss,plasma}$ was determined as the mean value of the plasma [^{3}H]pitavastatin concentrations at 60, 90, 120, 150, 180, and 210 min. V_{bile} was determined as the mean value of the biliary excretion rate of [^{3}H]pitavastatin from 60 to 90 min, from 90 to 120 min, from 120 to 150 min, from 150 to 180 min, and from 180 to 210 min. In mice, $C_{ss,plasma}$ was determined as the mean value of the plasma unlabeled pitavastatin concentrations at 90, 120, and 150 min. V_{bile} was determined as the mean value of the biliary excretion rate of unlabeled pitavastatin from 90 to 105 min, from 105 to 120 min, from 120 to 135 min, and from 135 to 150 min. $C_{ss,liver}$ was determined as the hepatic pitavastatin concentration at the end of the in vivo experiment. To calculate $C_{ss,liver}$, the specific gravity of the liver was assumed to be unity. Thus, the amount in the liver (nanograms per gram of liver) can be regarded as the hepatic concentration (nanograms per gram), and the units of $CL_{bile,liver}$ are in milliliters per minute per kilogram.

Statistical Analysis. Statistically significant differences were determined using one-way analysis of variance followed by Fisher's least significant difference method. Differences were considered to be significant at $P < 0.05$.

Results

ATP-Dependent Uptake of [^{3}H]Pitavastatin into BCRP-Expressing Membrane Vesicles. The time profiles and Eadie-Hofstee plots for the uptake of [^{3}H]pitavastatin by BCRP-expressing membrane vesicles are shown in Fig. 1. The uptake of [^{3}H]pitavastatin into membrane vesicles from human and mouse BCRP-transfected HEK293 cells was markedly stimulated by ATP but not that into GFP-transfected control cells (Fig. 1, A and B). The concentration-dependence of human and mouse BCRP-mediated ATP-dependent uptake of pitavastatin is shown in Fig. 1, C and D. The K_m and V_{max} values for the ATP-dependent uptake of pitavastatin were 5.73 ± 1.52 μM and 1106 ± 79 pmol/min/mg protein by human BCRP and 4.77 ± 0.50 μM and 881 ± 20 pmol/min/mg protein by mouse Bcrp, respectively.

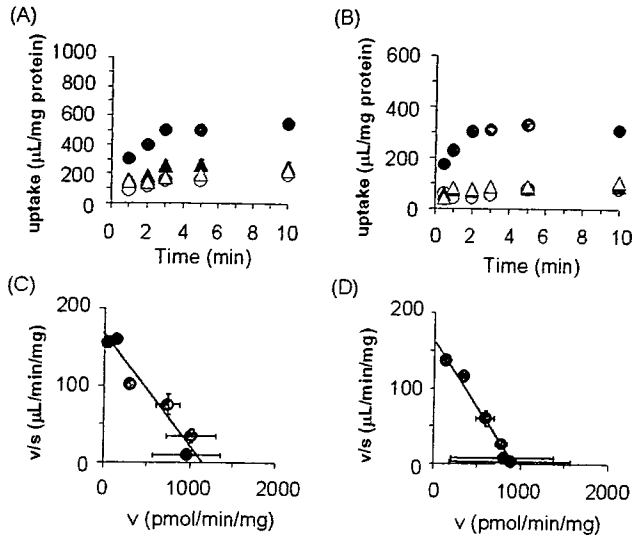

Fig. 1. Time profiles and Eadie-Hofstee plots of the uptake of [^{3}H]pitavastatin by human and mouse BCRP-expressing membrane vesicles. The uptake of 0.1 μM [^{3}H]pitavastatin by human BCRP (hBCRP) (A) and mouse Bcrp (mBcrp) (B), respectively, was examined at 37°C in medium containing 5 mM ATP (closed symbols) or AMP (open symbols). Circles and triangles represent the uptake in hBCRP- (or mBcrp-) and GFP-expressing membrane vesicles, respectively. The hBCRP- (C) and mBcrp (D)-mediated uptake of [^{3}H]pitavastatin was determined for 2 and 1 min, respectively. Each point represents the mean ± S.E. (n = 3). Where vertical bars are not shown, the S.E. values are within the limits of the symbols. The data were fitted to the Michaelis-Menten equation by nonlinear regression analysis, as described under *Materials and Methods*, and each solid line represents the fitted curve.

Uptake of Other Statins into BCRP-Expressing Membrane Vesicles. Uptake of other statins into human and mouse BCRP-expressing membrane vesicles was observed (Fig. 2). We did not see any significant ATP-dependent uptake of cerivastatin and fluvastatin by mouse Bcrp-expressing membrane vesicles compared with GFP-transfected vesicles, whereas human BCRP significantly recognized all of the statins we tested (cerivastatin, fluvastatin, pitavastatin, pravastatin, and rosuvastatin) as a substrate (Fig. 2, A–E). Estrone-3-sulfate (0.1 μM), which was a positive control compound for BCRP-mediated transport, was accepted as a substrate of both human and mouse BCRP (Fig. 2F). The K_m value of estrone-3-sulfate by mouse Bcrp was 16.4 ± 3.0 μM (data not shown).

Inhibitory Effects of Statins on the ATP-Dependent Uptake of [^{3}H]Estrone-3-sulfate into Human and Mouse BCRP-Expressing Membrane Vesicles. The inhibitory effects of statins on the ATP-dependent uptake of [^{3}H]estrone-3-sulfate by human and mouse BCRP-expressing membrane vesicles were observed. All of the statins except for pravastatin (~300 μM), inhibited the ATP-dependent uptake of [^{3}H]estrone-3-sulfate by human and mouse BCRP in a dose-dependent manner. The K_i values of statins for human and mouse BCRP are summarized in Table 1.

Transcellular Transport of Pitavastatin across Double Transfectants. Transcellular transport of pitavastatin across double-transfected MDCK II monolayers expressing uptake transporter (OATP1B1) and efflux transporter (MDR1, MRP2, or BCRP) was compared with that across the single-transfected monolayer and the vector-transfected con-

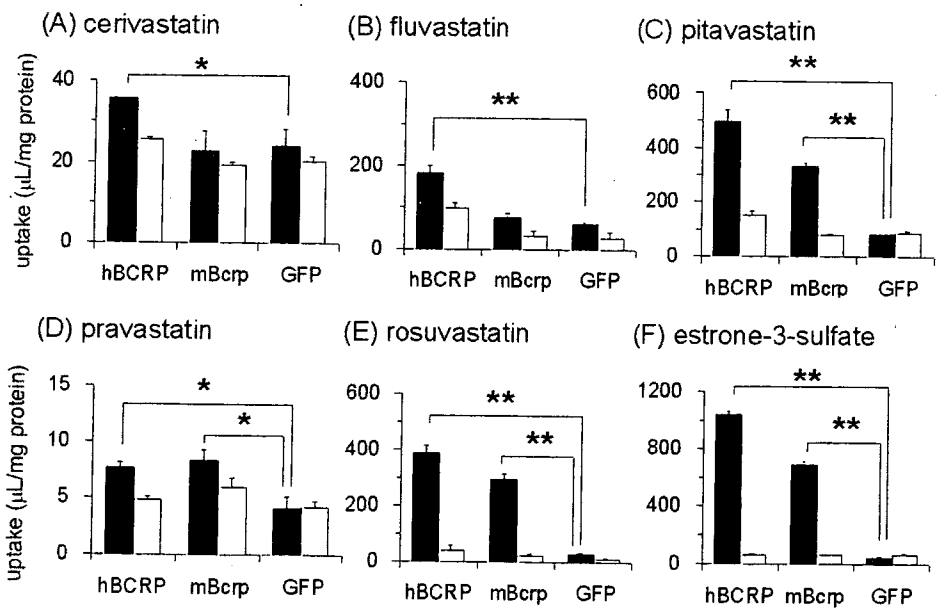

Fig. 2. The ATP-dependent uptake of statins by human BCRP (hBCRP)-, mouse Bcrp (mBcrp)-, and GFP-expressing membrane vesicles. The uptake of 0.1 μM [^{3}H]cerivastatin (A), 5 μM [^{14}C]fluvastatin (B), 0.1 μM [^{3}H]pitavastatin (C), 0.1 μM [^{3}H]pravastatin (D), and 0.1 μM [^{3}H]rosuvastatin (E) for 5 min and 0.1 μM [^{3}H]estrone-3-sulfate (F) for 2 min, respectively, was determined at 37°C in medium in the presence of 5 mM ATP (■) or AMP (□). Each point represents the mean ± S.E. (n = 3). *, $P < 0.05$; **, $P < 0.01$

trol monolayer. In the case of humans, as shown in Fig. 3, a symmetrical flux of pitavastatin was observed across the control, MDR1-, MRP2-, and BCRP-expressing MDCK II monolayer. The basal-to-apical flux of pitavastatin across the OATP1B1-expressing monolayer was approximately twice that in the opposite direction, whereas the basal-to-apical flux of pitavastatin was approximately 15, 110, and 230 times higher than that in the opposite direction in OATP1B1/MRP2, OATP1B1/BCRP, and OATP1B1/MDR1 double-transfected cells, respectively. In addition, transcellular transport of pitavastatin across double-transfected MDCK II monolayers expressing rat Oatp1b2 and Mrp2 was also compared with that across the Oatp1b2 or Mrp2 single-transfected monolayer and the vector-transfected control monolayer. The basal-to-apical flux of pitavastatin was 2.4 times higher than that in the opposite direction in the Oatp1b2/Mrp2 double-transfected cells, although a smaller vectorial transport was observed even in the Oatp1b2-expressing monolayer (Fig. 4). In both rats and humans, we checked the transcellular transport of $E_2 17\beta G$ as a positive control in parallel and obtained results similar to those measured previously (Matsushima et al., 2005; data not shown).

TABLE 1

Inhibitory effects of statins on the ATP-dependent uptake of [^{3}H]estrone-3-sulfate by human BCRP- and mouse Bcrp-expressing membrane vesicles

The ATP-dependent uptake of [^{3}H]estrone-3-sulfate (0.1 μM) for 1 min by human BCRP (hBCRP) and mouse Bcrp (mBcrp) was determined in the presence and absence of unlabeled statins at the designated concentrations. The values are expressed as a percentage of the ATP-dependent uptake of [^{3}H]estrone-3-sulfate in the absence of any unlabeled compounds. The ATP-dependent uptake was obtained by subtracting the transport velocity in the presence of AMP from that in the presence of ATP. The K_i values were determined by fitting the data using the non-least squares method. The values are expressed as mean ± computer-calculated S.D. (n = 3):

Statins	hBCRP	mBcrp
	μM	
Atorvastatin	14.3 ± 1.9	17.6 ± 1.7
Cerivastatin	18.1 ± 2.5	30.1 ± 6.3
Fluvastatin	5.43 ± 0.27	8.62 ± 0.86
Pitavastatin	2.92 ± 0.35	6.00 ± 0.71
Pravastatin	>300 μM	>300 μM
Rosuvastatin	15.4 ± 2.4	10.3 ± 0.6
Simvastatin acid	18.0 ± 4.3	24.9 ± 3.8

Plasma, Liver Concentration and Biliary Excretion Profiles at Steady State in Sprague-Dawley Rats and EHBRs. It has been reported that pitavastatin is not significantly metabolized in rats, and 70% of the excreted amount in bile can be detected in unchanged form (Fujino et al., 2002). Therefore, we used [^{3}H]pitavastatin in rats in an in vivo study to examine the involvement of Mrp2 in the biliary excretion of pitavastatin. The plasma concentration of pitavastatin reached a plateau at 60 min during constant infusion after a bolus intravenous administration. The biliary excretion rate (V_{bile}), the steady-state plasma concentration ($C_{ss,plasma}$), and total clearance (CL_{total}) values of pitavastatin in EHBRs were almost the same as those in normal rats (Fig. 5 and Table 2). The concentration of pitavastatin and the K_p value in the liver at steady state in EHBRs were lower than those in normal rats, and the $CL_{bile,plasma}$ and $CL_{bile,\ liver}$ values in EHBRs were slightly higher than those in normal rats, although the differences were not statistically significant (Fig. 5).

Plasma, Tissue Concentration, and Biliary Excretion Profiles at Steady State in FVB and Bcrp1(−/−) Mice. The plasma concentration of pitavastatin reached a plateau at 90 min during constant infusion (Fig. 6). The V_{bile} of parent pitavastatin in Bcrp1(−/−) mice was much lower than that in control mice, whereas the $C_{ss,plasma}$ and CL_{total} values of pitavastatin in Bcrp1(−/−) mice did not differ from those in normal mice (Table 3). The K_p values of pitavastatin in the kidney, brain, and skeletal muscle as well as the liver (Table 3) at steady state were similar in control and Bcrp1(−/−) mice (K_p value for kidney, 1.41 ± 0.10 and 1.48 ±0.12 ng/g; for brain, 0.0308 ± 0.0027 and 0.0322 ± 0.0070 ng/g; and for skeletal muscle, 0.0985 ± 0.0075 and 0.0960 ± 0.0061 ng/g in wild-type and Bcrp1(−/−) mice, respectively).

Discussion

Pitavastatin, a new potent inhibitor of HMG-CoA reductase, is scarcely metabolized in humans and is believed to be excreted into the bile in intact form. In the present study, we concentrated on a new candidate transporter, BCRP, for the biliary excretion of pitavastatin.

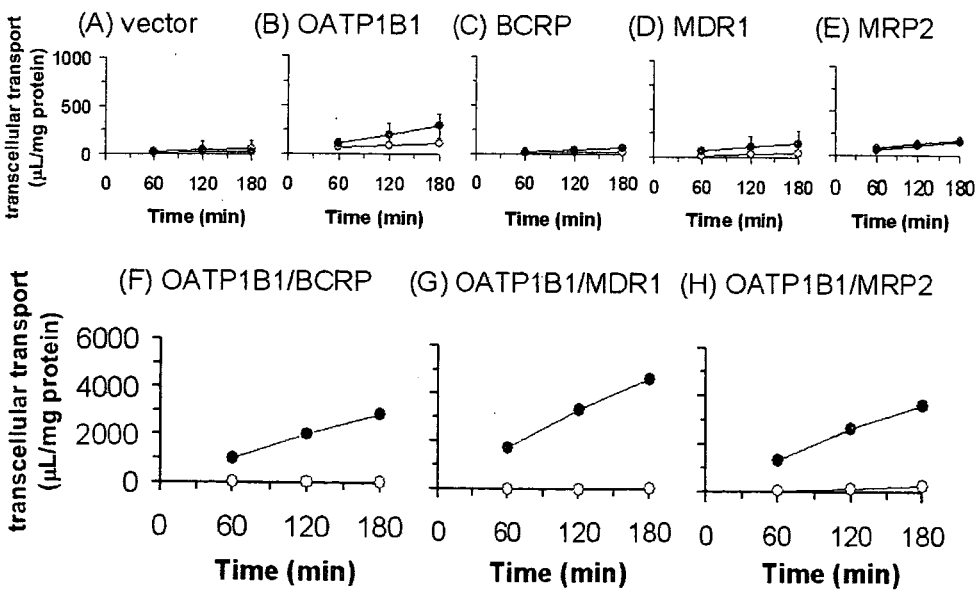

Fig. 3. Time profiles for the transcellular transport of [^{3}H]pitavastatin across MDCK II monolayers expressing human transporters. Transcellular transport of [^{3}H]pitavastatin (0.1 μM) across MDCK II monolayers expressing OATP1B1 (B), BCRP (C), MDR1 (D), MRP2 (E), both OATP1B1 and BCRP (F), both OATP1B1 and MDR1 (G), and both OATP1B1 and MRP2 (H) was compared with that across the vector-transfected control MDCK II monolayer (A). ○ and ● represent the transcellular transport in the apical-to-basal and basal-to-apical direction, respectively. Each point represents the mean ± S.E. (n = 3). Where vertical bars are not shown, the S.E. values are within the limits of the symbols.

ATP-dependent uptake of pitavastatin in human and mouse BCRP-expressing membrane vesicles was observed (Fig. 1). The K_m value of pitavastatin for human BCRP (5.73 μM) was almost the same as that for mouse Bcrp (4.77 μM), and these K_m values were similar to that of estrone-3-sulfate, which is a well-known substrate of human BCRP (Suzuki et al., 2003), indicating that pitavastatin is also a good substrate of BCRP. Regarding other statins, as shown in Table 1, no species difference in the K_i value of each statin for the BCRP-mediated uptake of estrone-3-sulfate was observed between humans and mice. The inhibition potency of statins, except for pravastatin, was almost identical, whereas pravastatin could not inhibit the BCRP-mediated transport of estrone-3-sulfate up to 300 μM. On the other hand, all statins we tested could be substrates of human BCRP, whereas four of them were also substrates of mouse Bcrp (Fig. 2). From a pharmacokinetic viewpoint, BCRP could at least partly contribute to the biliary excretion of pravastatin, pitavastatin, and rosuvastatin, which are scarcely metabolized by metabolic enzymes like cytochrome P450 in the liver. On the other hand, in the case of atorvastatin, cerivastatin, and simvastatin, which have been reported to be extensively metabolized by cytochrome P450 enzymes (Garcia et al., 2003), the biliary excretion of their unchanged form via BCRP was considered to be minor in in vivo situations.

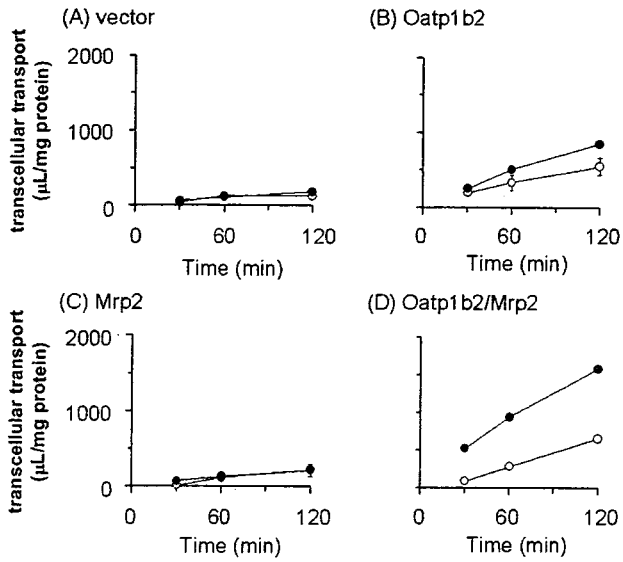

Fig. 4. Time profiles for the transcellular transport of [^{3}H]pitavastatin across MDCK II monolayers expressing rat transporters. Transcellular transport of [^{3}H]pitavastatin (0.1 μM) across MDCK II monolayers expressing Oatp1b2 (B), Mrp2 (C), and both Oatp1b2 and Mrp2 (D) was compared with that across the vector-transfected control MDCK II monolayer (A). ○ and ● represent the transcellular transport in the apical-to-basal and basal-to-apical direction, respectively. Each point represents the mean ± S.E. (n = 3). Where vertical bars are not shown, the S.E. values are within the limits of the symbols.

To estimate the contribution of each transporter to the biliary excretion of pitavastatin in the in vivo study, the biliary excretion of pitavastatin at steady state was investigated using Mrp2- and Bcrp1-deficient animals. Because pitavastatin was found to be scarcely metabolized in rats (Fujino et al., 2002), the radioactivity would reflect the parent pitavastatin. We confirmed that the plasma concentration and biliary excretion rate of pitavastatin was not changed between Sprague-Dawley rats and EHBRs (Fig. 5 and Table. 2), which is consistent with a previous report (Fujino et al., 2002). Therefore, the involvement of Mrp2 in the biliary excretion of pitavastatin is minor. The liver concentration in EHBRs was significantly lower than that in control rats possibly because of the accelerated efflux via the basolateral membrane in the liver caused by the induction of Mrp3 (Ogawa et al., 2000) and the inhibition of hepatic uptake process from the blood by a higher concentration of bilirubin glucuronide in EHBRs (Sathirakul et al., 1993), or by the decrease in the expression levels of transporters responsible for the uptake of pitavastatin.

Biliary excretion of pitavastatin was also observed in Bcrp1(−/−) and control mice. In contrast to humans and rats, pitavastatin is extensively metabolized in mice, so we decided to quantify the unchanged form separately by LC/MS in mice. The biliary excretion clearance of pitavastatin in Bcrp1(−/−) mice was 10 times lower than that in control mice, suggesting that unchanged pitavastatin is excreted into bile mainly by Bcrp. In control mice, the biliary clear-

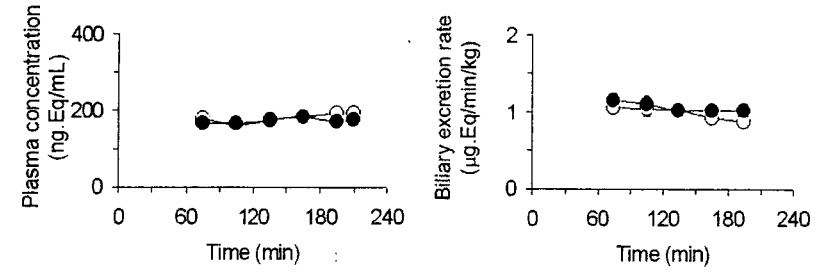

Fig. 5. Plasma concentrations and biliary excretion rate of [^{3}H]pitavastatin during constant intravenous infusion into Sprague-Dawley rats and EHBRs. The plasma concentration (A) and biliary excretion rate (B) of total radioactivity were determined during constant intravenous infusion into Sprague-Dawley rats (○) and EHBRs (●). Each point plotted, with its vertical bar, represents the mean ± S.E. of four rats.

TABLE 2

Pharmacokinetic parameters of pitavastatin during constant intravenous infusion into Sprague-Dawley (SD) rats and EHBRs

Data represent the mean ± S.E. (n = 4).

	$C_{ss,plasma}$	CL_{total}	$CL_{bile,plasma}$	$CL_{bile,liver}$	Liver Concentration	$K_{p,liver}$
	ng · Eq/ml	*ml/min/kg*	*ml/min/kg*	*ml/min/kg*	*ng · Eq/g*	
SD rat	195 ± 13	6.26 ± 0.49	4.55 ± 0.13	0.248 ± 0.042	4346 ± 406	23.0 ± 3.6
EHBR	179 ± 8	6.75 ± 0.34	5.77 ± 0.53	0.399 ± 0.049	2621 ± 139**	14.7 ± 0.8

** $P < 0.01$.

$C_{ss,plasma}$, plasma steady-state concentration (mean of plasma concentration at 210 min); CL_{total}, total plasma clearance obtained by dividing the infusion rate by $C_{ss,plasma}$; $CL_{bile,plasma}$, biliary clearance normalized by the plasma concentration; $CL_{bile,liver}$, biliary clearance normalized by the liver concentration; $K_{p,liver}$, K_p value obtained by dividing the liver concentration by $C_{ss,plasma}$ (at 210 min).

ance normalized by plasma concentration ($CL_{bile,plasma}$) accounted for only 5% of the plasma total clearance (CL_{total}), indicating that pitavastatin is mainly excreted into bile as metabolites. Taking extensive metabolism into consideration, it is natural that the plasma and liver concentrations were not different between Bcrp1(−/−) and control mice, even if the biliary clearance of the parent compound was drastically reduced in Bcrp1(−/−) mice. In contrast to mice, pitavastatin is believed to be excreted into the bile in an intact form with only minimal metabolism in humans (Fujino et al., 2003). Therefore, BCRP is estimated to be involved in the biliary excretion of pitavastatin in humans. On the other hand, a previous in vivo study using EHBRs revealed that Mrp2 is a major transporter for the excretion of pravastatin in rats (Yamazaki et al., 1997). Even though pitavastatin and pravastatin belong to the same category, HMG-CoA reductase inhibitors, it was interesting to find that pitavastatin and pravastatin are excreted into the bile by different efflux transport systems. In the brain and kidney, in which BCRP is also expressed, and skeletal muscle, which is a target site of severe adverse effects of statins (rhabdomyolysis), these tissue concentrations were not significantly different between Bcrp1(−/−) and control mice. Thus, Bcrp does not contribute to the distribution of pitavastatin in these tissues. BCRP was expressed not only in the liver, kidney, and brain, but also in the small intestine and mammary gland (Doyle and Ross, 2003). It has been demonstrated that BCRP critically modulates the absorption of certain drugs from the small intestine and transfer to milk (Adachi et al., 2004; Merino et al., 2005a). Further studies are needed to clarify the importance of BCRP in the intestinal absorption and tissue distribution of a series of statins.

In Fig. 3, we clearly observed the vectorial basal-to-apical transport of pitavastatin across all of the double transfectants (OATP1B1/BCRP, OATP1B1/MDR1, and OATP1B1/MRP2) in contrast to that across the control and OATP1B1 single-transfected cells. The efflux transport clearance of pitavastatin normalized by the intracellular concentration did not differ much among MDR1, MRP2, and BCRP, the range being only 2-fold. In the case of pravastatin, we demonstrated previously that the efflux clearance of MRP2 was much higher than that of MDR1 and BCRP (Matsushima et al., 2005). Considering these facts, the relative contribution of MDR1 and BCRP to the biliary excretion of pitavastatin was larger than that of pravastatin. In the case of rats, the basal-to-apical flux of pitavastatin across the Oatp1b2/Mrp2 double transfectants was significantly higher than that across the Oatp1b2 single transfectants (Fig. 4). However, the ratio of basal-to-apical to apical-to-basal flux of pitavastatin in Oatp1b2/Mrp2 double-transfected cells divided by that in Oatp1b2 single-transfected cells was approximately 1.6, which was small in comparison with that of other substrates tested previously (Sasaki et al., 2004). Therefore, although pitavastatin is a substrate of rat Mrp2, the intrinsic efflux clearance of pitavastatin via rat Mrp2 seems to be relatively low.

The elimination of diflomotecan from plasma has been found to be delayed in patients with frequently observed SNP in BCRP (C421A/Q141K) (Sparreboom et al., 2004). Various reports suggested that this SNP affected the protein expression level of BCRP in the placenta without changing its intrinsic efflux clearance (Kondo et al., 2004; Kobayashi et al., 2005). On the other hand, both in vivo and in vitro studies revealed that the frequently observed haplotype OATP1B1*15 (N130D and V174A) reduced the nonrenal clearance of pravastatin (Nishizato et al., 2003; Iwai et al., 2004). We demonstrated previously that pitavastatin is taken up into hepatocytes mainly by OATP1B1 (Hirano et al., 2004). Taking these facts into consideration, further clinical studies are needed to investigate the effect of SNPs in OATP1B1 and BCRP on the pharmacokinetics of pitavastatin and to determine the importance of each transporter directly in humans.

In the present study, we have shown that pitavastatin is recognized by human and mouse BCRP in expression systems, and Bcrp is mainly involved in the biliary excretion of pitavastatin by knockout animals. BCRP can also accept other statins as a substrate, implying that it is important to

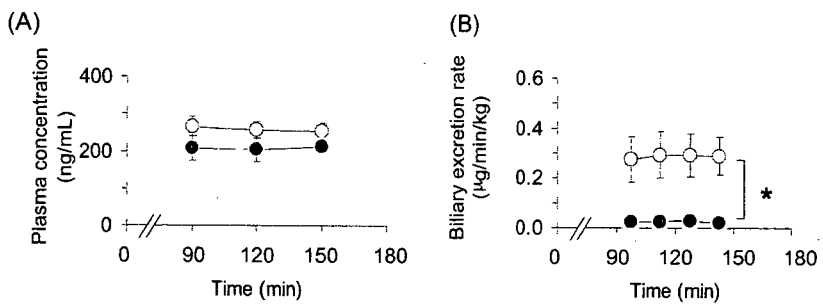

Fig. 6. Plasma concentration and biliary excretion rate of pitavastatin during constant intravenous infusion into wild-type and Bcrp1(−/−) mice. The plasma concentration (A) and biliary excretion rate (B) of pitavastatin were determined during constant intravenous infusion into wild-type (○) and Bcrp1(−/−) (●) mice. Each point plotted, with its vertical bar, represents the mean ± S.E. of four mice. *, $P < 0.05$

TABLE 3

Pharmacokinetic parameters of pitavastatin during constant intravenous infusion into wild-type and Bcrp1(−/−) mice

Data represent the mean ± S.E. ($n = 4$).

	$C_{ss,plasma}$	CL_{total}	$CL_{bile,plasma}$	$CL_{bile,liver}$	Liver Concentration	$K_{p,liver}$
	ng/ml	*ml/min/kg*	*ml/min/kg*	*ml/min/kg*	*ng/g*	
Wild type	254 ± 21	20.1 ± 1.8	1.21 ± 0.43	0.364 ± 0.032	813 ± 196	3.34 ± 1.03
Bcrp1(−/−)	213 ± 22	24.2 ± 2.5	0.110 ± 0.02*	0.0293 ± 0.0036**	798 ± 124	3.94 ± 0.83

* $P < 0.05$; ** $P < 0.01$.

$C_{ss,plasma}$, plasma steady-state concentration (mean of plasma concentration at 150 min); CL_{total}, total plasma clearance obtained by dividing the infusion rate by $C_{ss,plasma}$; $CL_{bile,plasma}$, biliary clearance normalized by the plasma concentration; $CL_{bile,liver}$, biliary clearance normalized by the liver concentration; $K_{p,liver}$, K_p value obtained by dividing the liver concentration by $C_{ss,plasma}$ (at 150 min).

estimate how the change of function and expression level of BCRP affects the pharmacokinetics of statins. In humans, because it is evident that pitavastatin is a substrate of BCRP, MDR1, and MRP2 by double transfectants, it will be important to estimate the contribution of each transporter to the biliary excretion of pitavastatin in humans.

Acknowledgments

We thank Dr. Alfred H Schinkel (The Netherlands Cancer Institute, the Netherlands) and Dr. Johan A Jonker (The Salk Institute for Biological Studies, San Diego, CA) for constructing Bcrp1(−/−) mice and giving us valuable comments, Dr. Piet Borst (The Netherlands Cancer Institute) for providing the MDCK II cells expressing MRP2 and MDR1, and Dr. Yoshihiro Miwa (University of Tsukuba, Tsukuba, Japan) for providing pEB6CAGMCS/SRZeo vector. We also thank Dr. Makoto Sasaki for constructing Oatp1b2/Mrp2 double-transfected cells and Chihiro Kondo for constructing human BCRP recombinant adenovirus. We also thank Sankyo Co., Ltd. (Tokyo, Japan) for providing radiolabeled pravastatin, Novartis Pharma K.K. (Basel, Switzerland) for providing radiolabeled fluvastatin, AstraZeneca PLC (London, UK), for providing radiolabeled rosuvastatin, and Kowa Co. Ltd. (Tokyo, Japan) for providing radiolabeled pitavastatin and unlabeled statins.

References

Adachi Y, Suzuki H, Schinkel AH, and Sugiyama Y (2004) Role of breast cancer resistance protein (Bcrp1/Abcg2) in the extrusion of glucuronide and sulfate conjugates from enterocytes to intestinal lumen. *Mol Pharmacol* **67**:923–928.

Allikmets R, Schriml LM, Hutchinson A, Romano-Spica V, and Dean M (1998) A human placenta-specific ATP-binding cassette gene (ABCP) on chromosome 4q22 that is involved in multidrug resistance. *Cancer Res* **58**:5337–5339.

Chandra P and Brouwer KL (2004) The complexities of hepatic drug transport: current knowledge and emerging concepts. *Pharm Res (NY)* **21**:719–735.

Cvetkovic M, Leake B, Fromm MF, Wilkinson GR, and Kim RB (1999) OATP and P-glycoprotein transporters mediate the cellular uptake and excretion of fexofenadine. *Drug Metab Dispos* **27**:866–871.

Doyle LA and Ross DD (2003) Multidrug resistance mediated by the breast cancer resistance protein BCRP (ABCG2). *Oncogene* **22**:7340–7358.

Fujino H, Saito T, Tsunenari Y, and Kojima J (2003) Interaction between several medicines and statins. *Arzneimittelforschung* **53**:145–153.

Fujino H, Yamada I, Shimada S, and Kojima J (2002) Metabolic fate of pitavastatin, a new inhibitor of HMG-CoA reductase-effect of cMOAT deficiency on hepatobiliary excretion in rats and of mdr1a/b gene disruption on tissue distribution in mice. *Drug Metab Pharmacokinet* **17**:449–456.

Garcia MJ, Reinoso RF, Sanchez Navarro A, and Prous JR (2003) Clinical pharmacokinetics of statins. *Methods Find Exp Clin Pharmacol* **25**:457–481.

Hirano M, Maeda K, Hayashi H, Kusuhara H, and Sugiyama Y (2005) Bile salt export pump (BSEP/ABCB11) can transport a nonbile acid substrate, pravastatin. *J Pharmacol Exp Ther* **314**:876–882.

Hirano M, Maeda K, Shitara Y, and Sugiyama Y (2004) Contribution of OATP2 (OATP1B1) and OATP8 (OATP1B3) to the hepatic uptake of pitavastatin in humans. *J Pharmacol Exp Ther* **311**:139–146.

Hirohashi T, Suzuki H, and Sugiyama Y (1999) Characterization of the transport properties of cloned rat multidrug resistance-associated protein 3 (MRP3). *J Biol Chem* **274**:15181–15185.

Imai Y, Nakane M, Kage K, Tsukahara S, Ishikawa E, Tsuruo T, Miki Y, and Sugimoto Y (2002) C421A polymorphism in the human breast cancer resistance protein gene is associated with low expression of Q141K protein and low-level drug resistance. *Mol Cancer Ther* **1**:611–616.

Iwai M, Suzuki H, Ieiri I, Otsubo K, and Sugiyama Y (2004) Functional analysis of single nucleotide polymorphisms of hepatic organic anion transporter OATP1B1 (OATP-C). *Pharmacogenetics* **14**:749–757.

Jonker JW, Buitelaar M, Wagenaar E, Van Der Valk MA, Scheffer GL, Scheper RJ, Plosch T, Kuipers F, Elferink RP, Rosing H, et al. (2002) The breast cancer resistance protein protects against a major chlorophyll-derived dietary phototoxin and protoporphyria. *Proc Natl Acad Sci USA* **99**:15649–15654.

Jonker JW, Smit JW, Brinkhuis RF, Maliepaard M, Beijnen JH, Schellens JH, and Schinkel AH (2000) Role of breast cancer resistance protein in the bioavailability and fetal penetration of topotecan. *J Natl Cancer Inst* **92**:1651–1656.

Kajinami K, Takekoshi N, and Saito Y (2003) Pitavastatin: efficacy and safety profiles of a novel synthetic HMG-CoA reductase inhibitor. *Cardiovasc Drug Rev* **21**:199–215.

Kimata H, Fujino H, Koide T, Yamada Y, Tsunenari Y, Yonemitsu M, and Yanagawa Y (1998) Studies on the metabolic fate of NK-104, a new inhibitor of HMG-CoA reductase: I. Absorption, distribution, metabolism and excretion in rats. *Xenobiol Metab Dispos* **13**:484–498.

Kobayashi D, Ieiri I, Hirota T, Takane H, Maegawa S, Kigawa J, Suzuki H, Nanba E, Oshimura M, Terakawa N, et al. (2005) Functional assessment of ABCG2 (BCRP) gene polymorphisms to protein expression in human placenta. *Drug Metab Dispos* **33**:94–101.

Kojima J, Ohshima T, Yoneda M, and Sawada H (2001) Effect of biliary excretion on the pharmacokinetics of pitavastatin (NK-104) in dogs. *Xenobio Metab Dispos* **16**:497–502.

Kondo C, Onuki R, Kusuhara H, Suzuki H, Suzuki M, Okudaira N, Kojima M, Ishiwata K, Jonker JW, and Sugiyama Y (2005) Lack of improvement of oral absorption of ME3277 by prodrug formation is ascribed to the intestinal efflux mediated by breast cancer resistant protein (BCRP/ABCG2). *Pharm Res (NY)* **22**:613–618.

Kondo C, Suzuki H, Itoda M, Ozawa S, Sawada J, Kobayashi D, Ieiri I, Mine K, Ohtsubo K, and Sugiyama Y (2004) Functional analysis of SNPs variants of BCRP/ABCG2. *Pharm Res (NY)* **21**:1895–1903.

Kruijtzer CM, Beijnen JH, Rosing H, ten Bokkel Huinink WW, Schot M, Jewell RC, Paul EM, and Schellens JH (2002) Increased oral bioavailability of topotecan in combination with the breast cancer resistance protein and P-glycoprotein inhibitor GF120918. *J Clin Oncol* **20**:2943–2950.

Maliepaard M, Scheffer GL, Faneyte IF, van Gastelen MA, Pijnenborg AC, Schinkel AH, van De Vijver MJ, Scheper RJ, and Schellens JH (2001) Subcellular localization and distribution of the breast cancer resistance protein transporter in normal human tissues. *Cancer Res* **61**:3458–3464.

Matsushima S, Maeda K, Kondo C, Hirano M, Sasaki M, Suzuki H, and Sugiyama Y (2005) Identification of the hepatic efflux transporters of organic anions using double-transfected Madin-Darby canine kidney II cells expressing human organic anion-transporting polypeptide 1B1 (OATP1B1)/multidrug resistance-associated protein 2, OATP1B1/multidrug resistance 1, and OATP1B1/breast cancer resistance protein. *J Pharmacol Exp Ther*, in press.

Merino G, Jonker JW, Wagenaar E, van Herwaarden AE, and Schinkel AH (2005a) The Breast Cancer Resistance Protein (BCRP/ABCG2) affects pharmacokinetics, hepatobiliary excretion and milk secretion of the antibiotic nitrofurantoin. *Mol Pharmacol* **65**:1758–1764.

Merino G, van Herwaarden AE, Wagenaar E, Jonker JW, and Schinkel AH (2005b) Sex-dependent expression and activity of the ABC transporter Breast Cancer Resistance Protein (BCRP/ABCG2) in liver. *Mol Pharmacol* **67**:1765–1771.

Mizuno N, Suzuki M, Kusuhara H, Suzuki H, Takeuchi K, Niwa T, Jonker JW, and Sugiyama Y (2004) Impaired renal excretion of 6-hydroxy-5,7-dimethyl-2-methylamino-4-(3-pyridylmethyl) benzothiazole (E3040) sulfate in breast cancer resistance protein (BCRP1/ABCG2) knockout mice. *Drug Metab Dispos* **32**:898–901.

Muller M, Meijer C, Zaman GJ, Borst P, Scheper RJ, Mulder NH, de Vries EG, and Jansen PL (1994) Overexpression of the gene encoding the multidrug resistance-associated protein results in increased ATP-dependent glutathione S-conjugate transport. *Proc Natl Acad Sci USA* **91**:13033–13037.

Nishizato Y, Ieiri I, Suzuki H, Kimura M, Kawabata K, Hirota T, Takane H, Irie S, Kusuhara H, Urasaki Y, et al. (2003) Polymorphisms of OATP-C (SLC21A6) and OAT3 (SLC22A8) genes: consequences for pravastatin pharmacokinetics. *Clin Pharmacol Ther* **73**:554–565.

Ogawa K, Suzuki H, Hirohashi T, Ishikawa T, Meier PJ, Hirose K, Akizawa T, Yoshioka M, and Sugiyama Y (2000) Characterization of inducible nature of MRP3 in rat liver. *Am J Physiol* **278**:G438–G446.

Sasaki M, Suzuki H, Aoki J, Ito K, Meier PJ, and Sugiyama Y (2004) Prediction of in vivo biliary clearance from the in vitro transcellular transport of organic anions across a double-transfected Madin-Darby canine kidney II monolayer expressing both rat organic anion transporting polypeptide 4 and multidrug resistance associated protein 2. *Mol Pharmacol* **66**:450–459.

Sasaki M, Suzuki H, Ito K, Abe T, and Sugiyama Y (2002) Transcellular transport of organic anions across a double-transfected Madin-Darby canine kidney II cell monolayer expressing both human organic anion-transporting polypeptide (OATP2/SLC21A6) and Multidrug resistance-associated protein 2 (MRP2/ABCC2). *J Biol Chem* **277**:6497–6503.

Sathirakul K, Suzuki H, Yasuda K, Hanano M, Tagaya O, Horie T, and Sugiyama Y (1993) Kinetic analysis of hepatobiliary transport of organic anions in Eisai hyperbilirubinemic mutant rats. *J Pharmacol Exp Ther* **265**:1301–1312.

Sparreboom A, Gelderblom H, Marsh S, Ahluwalia R, Obach R, Principe P, Twelves C, Verweij J, and McLeod HL (2004) Diflomotecan pharmacokinetics in relation to ABCG2 421C>A genotype. *Clin Pharmacol Ther* **76**:38–44.

Stein EA, Lane M, and Laskarzewski P (1998) Comparison of statins in hypertriglyceridemia *Am J Cardiol* **26**;81 66B–89B.

Suzuki M, Suzuki H, Sugimoto Y, and Sugiyama Y (2003) ABCG2 transports sulfated conjugates of steroids and xenobiotics. *J Biol Chem* **278**:22644–22649.

van Herwaarden AE, Jonker JW, Wagenaar E, Brinkhuis RF, Schellens JH, Beijnen JH, and Schinkel AH (2003) The breast cancer resistance protein (Bcrp1/Abcg2) restricts exposure to the dietary carcinogen 2-amino-1-methyl-6-phenylimidazo[4,5-b]pyridine. *Cancer Res* **63**:6447–6452.

Yamaoka K, Tanigawara Y, Nakagawa T, and Uno T (1981) A pharmacokinetic analysis program (multi) for microcomputer. *J Pharmacobiodyn* **4**:879–885.

Yamazaki M, Akiyama S, Ni'inuma K, Nishigaki R, and Sugiyama Y (1997) Biliary excretion of pravastatin in rats: contribution of the excretion pathway mediated by canalicular multispecific organic anion transporter. *Drug Metab Dispos* **25**:1123–1129.

Zamber CP, Lamba JK, Yasuda K, Farnum J, Thummel K, Schuetz JD, and Schuetz EG (2003) Natural allelic variants of breast cancer resistance protein (BCRP) and their relationship to BCRP expression in human intestine. *Pharmacogenetics* **13**:19–28.

Address correspondence to: Dr. Yuichi Sugiyama, Department of Molecular Pharmacokinetics, Graduate School of Pharmaceutical Sciences, The University of Tokyo, 7-3-1 Hongo, Bunkyo-ku, Tokyo, 113-0033 Japan. E-mail: sugiyama@mol.f.u-tokyo.ac.jp

Pharmaceutical Research, Vol. 22, No. 2, February 2005 (© 2005)
DOI: 10.1007/s01869-005-1869-8

Research Paper

Estimation of the Three-Dimensional Pharmacophore of Ligands for Rat Multidrug-Resistance–Associated Protein 2 Using Ligand-Based Drug Design Techniques

Shuichi Hirono,[1,3] Izumi Nakagome,[1] Rie Imai,[1] Kazuya Maeda,[2] Hiroyuki Kusuhara,[2] and Yuichi Sugiyama[2]

Received March 22, 2004; accepted July 19, 2004

Purpose. Multidrug-resistance–associated protein 2 (Mrp2) shows a broad substrate specificity toward amphiphilic organic anions. This study identified key functional groups of ligand molecules for binding to rat Mrp2, determined their relative locations, and examined substrate specificity through receptor mapping using three-dimensional (3D) quantitative structure-activity relationship (3D-QSAR) analysis.
Methods. Ligand-binding conformations were estimated using conformational analysis (CAMDAS) and molecular superposition (SUPERPOSE) methods to clarify the substrate specificity of rat Mrp2 in relation to 3D ligand structures.
Results. Two types of binding conformations of ligands for rat Mrp2 were identified. 3D-QSAR comparative molecular-field analysis (CoMFA) revealed a statistically significant model for one type, in which the steric, electrostatic, and log P contributions to the binding affinity for rat Mrp2 were 63.0%, 33.4%, and 3.6%, respectively ($n = 16$, $q^2 = 0.59$, $n = 3$, $r^2 = 0.99$, and $s = 0.08$).
Conclusions. The 3D pharmacophore of ligands for rat Mrp2, and the ligand-binding region of rat Mrp2, were estimated. Ligand recognition of rat Mrp2 is achieved through interactions in two hydrophobic and two electrostatically positive sites (primary binding sites). The broad substrate specificity of rat Mrp2 might result from the combination of secondary (two electrostatically positive and two electrostatically negative sites) and primary binding sites.

KEY WORDS: binding conformation; 3D pharmacophore; 3D-QSAR; rat Mrp2; substrate specificity.

INTRODUCTION

The liver is one of the most important organs in the detoxification of xenobiotics, and biliary excretion is a major pathway for their elimination. Compounds in the circulating blood are taken up by hepatocytes and are then metabolized and/or excreted into the bile. Many kinds of drugs and their metabolites are transported across the sinusoidal and bile canalicular membranes via carriers. The mechanism of transport across the bile canalicular membrane has been characterized using isolated canalicular membrane vesicles (CMVs), which revealed that several types of primary active transporters are responsible for ligand efflux from the hepatocytes into the bile. Among them, multidrug-resistance–associated protein-2 (Mrp2; gene symbol ABCC2) has an important role in the biliary excretion of many organic anions and glutathione or glucuronide conjugates (1–3).

Mrp2 is an ATP-binding cassette (ABC) transporter, which possesses two highly conserved ABC regions. The Eisai hyperbilirubinemic rat (EHBR), which has a hereditary Mrp2 deficiency owing to the insertion of a nonsense mutation (4), and the GY/TR$^-$ rat (5) have both helped to reveal the importance of Mrp2 in the biliary excretion of various types of organic anions. In the EHBR, the biliary excretion of Mrp2 substrates is drastically decreased, and the ATP-dependent uptake of Mrp2 substrates into CMVs prepared from EHBRs is greatly reduced compared with those prepared from normal rats.

These findings demonstrate that a wide range of organic anions can be substrates for Mrp2, which include: nonconjugated organic anions such as dibromosulfophthalein (6,7), cefodizime (β-lactam antibiotic) (7), pravastatin (a 3-hydroxy-3-methyl-glutaryl-coenzyme A reductase inhibitor) (8), temocaprilat (an angiotensin-converting enzyme inhibitor) (9), the carboxylate forms of CPT-11 and its active metabolite (SN-38, which is a topoisomerase inhibitor) (8), and a cyclic anionic peptide (BQ-123, which is an endothelin antagonist) (10); glutathione conjugates such as leukotriene C_4 (11) and DNP-SG (12); and glucuronide conjugates such as bilirubin glucuronide (13), E3040 glucuronide (14,15), and SN-38 glucuronide (16).

[1] School of Pharmaceutical Sciences, Kitasato University, Tokyo 108-8641, Japan.
[2] Graduate School of Pharmaceutical Sciences, University of Tokyo, Tokyo 113-0033, Japan.
[3] To whom correspondence should be addressed. (e-mail: hironos@pharm.kitasato-u.ac.jp)

ABBREVIATIONS: ABC, ATP-binding cassette; CAMDAS, Conformational Analyzer with Molecular Dynamics and Sampling; C log P, calculated log P; CMVs, canalicular membrane vesicles; CoMFA, comparative molecular-field analysis; EHBR, Eisai hyperbilirubinemic rat; MD, molecular dynamics; Mrp2, multidrug-resistance–associated protein 2; PLS, partial least squares; QSAR, quantitative structure-activity relationship; rmsd, root-mean-square deviation; SD, Sprague-Dawley.

Clearly, rat Mrp2 accepts many organic anions as substrates. However, its broad substrate specificity has not been investigated in terms of the three-dimensional (3D) structures of ligands (17), and the complete 3D structure has not been determined for any mammalian transporter. Elucidating the structural characteristics of the ligand-binding region of rat Mrp2 would be useful for understanding its broad substrate specificity. Therefore, in the current study, we investigated the binding conformation of ligands to rat Mrp2, the key functional groups for binding to Mrp2 (3D pharmacophore), and the 3D quantitative structure-activity relationships (3D-QSAR) between ligands and rat Mrp2. Our combined method comprised the following three procedures: first, conformational analysis (CAMDAS) (18); second, a molecular superposition procedure (SUPERPOSE) (19); and third, 3D-QSAR analysis by comparative molecular-field analysis (CoMFA) (20). These techniques are described in more detail in the following section.

MATERIALS AND METHODS

Conformational Analysis: Sampling of a Set of Conformers of a Molecule

X-ray structural analysis of protein-ligand complexes has revealed that the binding conformation is one of the stable conformations of a ligand molecule. To generate a set of conformers of ligands, we used the automated program Conformational Analyzer with Molecular Dynamics and Sampling (CAMDAS), which was developed by Tsujishita and Hirono (18). CAMDAS performs high-temperature molecular dynamics (MD) calculations for a target molecule and for sampled conformers that appear during the MD. It then evaluates the similarities between each of the sampled conformers in terms of dihedral angle values, clusters similar conformers together, and, finally, prints out the clustered conformers. In this way, CAMDAS can find the representative conformers from an arbitrarily given structure of the molecule.

To estimate the binding conformation of ligands to rat Mrp2, MD dynamics calculations were executed for 18 ligands (a training set for constructing QSAR models comprising compounds **1–16** and a test set for verifying the QSAR models comprising compounds **A** and **B**), and many conformers were sampled; their chemical structures are shown in Figs. 1 and 2. An MD calculation for sampling was performed for 800 ps with an integral time step of 0.001 ps using an MM2 force field (21) without electrostatic and hydrogen-bonding interactions. The temperature of the system was maintained at 1200 K, and the length of the covalent bonds was fixed using the SHAKE algorithm throughout the MD simulations. Conformers were sampled at every 100 steps and preclustered with dihedral angles during the MD simulations. If the difference between conformers was within ±30°, they were grouped together. Subsequently, reclustering of the sampled conform-

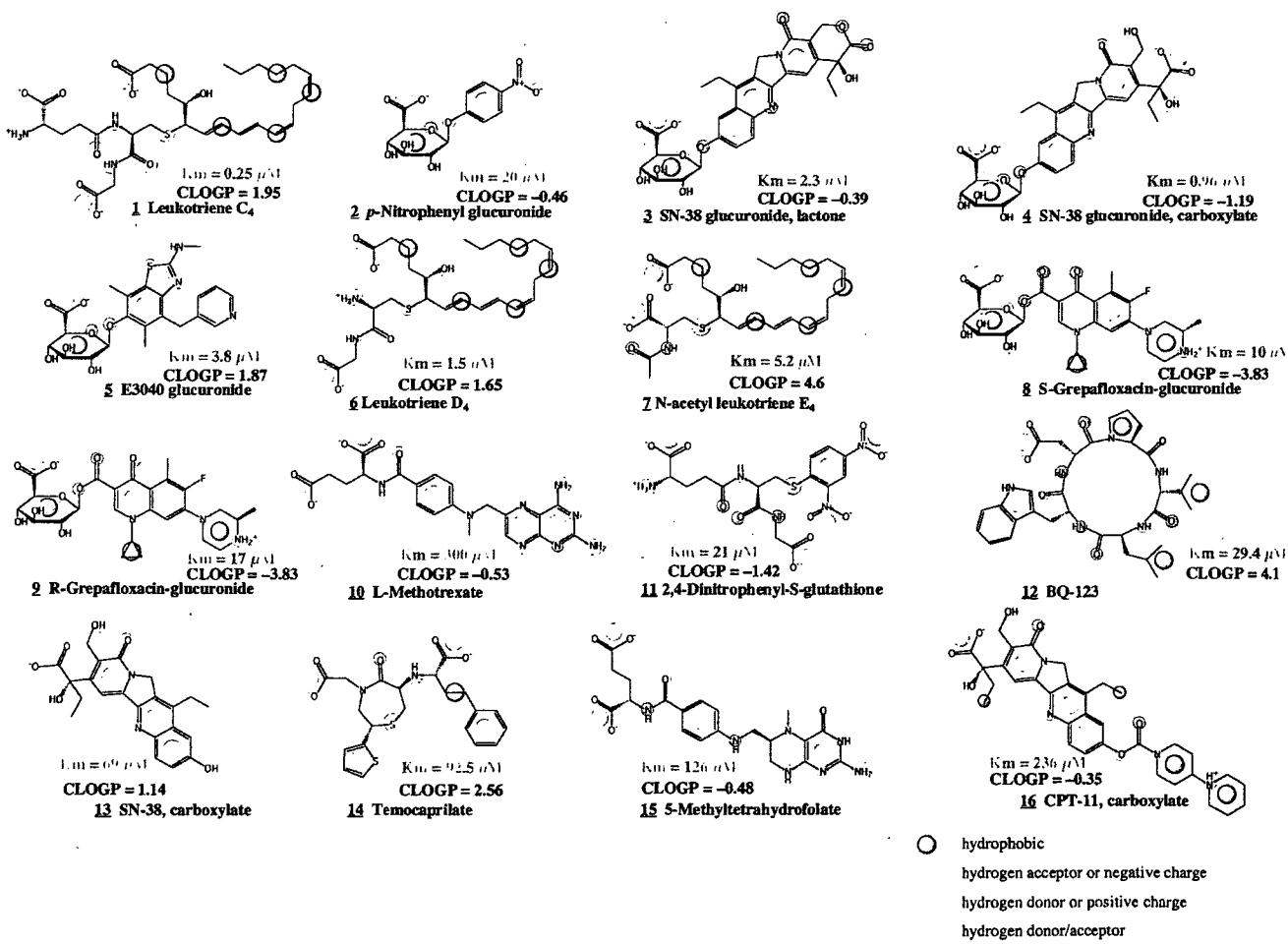

Fig. 1. Chemical structures of the compounds in the training set, with property spheres, K_m, and C log P values.

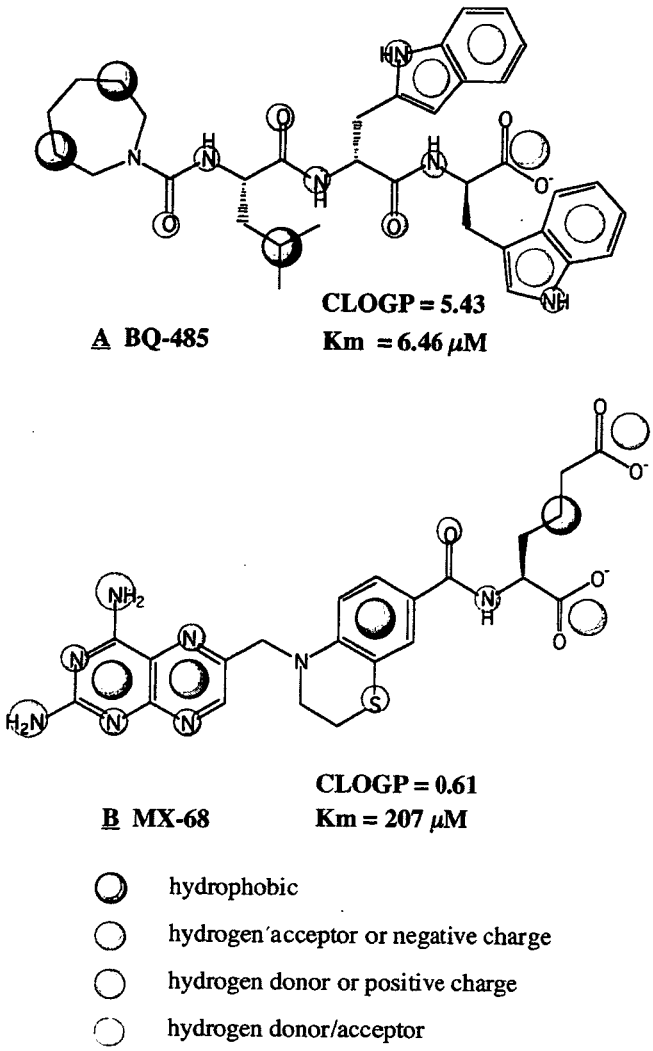

Fig. 2. Chemical structures of the compounds in the test set, with property spheres, K_m, and C log P values.

ers was performed with dihedral angles within ±30°. Before the clustering, each conformer was minimized until the root-mean-square (rms) of the gradients of the potential energy was below 0.004 kcal mol^{-1} $Å^{-1}$.

Molecular Superposition: Selection of the Candidate Binding Conformations

X-ray crystallographic studies of protein-ligand complexes have demonstrated that when ligands bind to a given protein, such as a receptor or a transporter, the atomic groups in the ligands that interact with amino-acid residues of the protein occupy the same 3D space. Based on this information, we carried out molecular superposition for ligand molecules using the SUPERPOSE program developed by Iwase and Hirono (19). The program superposes two molecules based on the physicochemical properties of the atomic groups, which is useful for elucidating a pharmacophore and estimating a binding conformation by distinguishing it from among the many conformations that are generated by high-temperature MD calculations.

Five types of physicochemical properties are considered in the program, including hydrophobic (aromatic), hydrogen-bond donors, hydrogen-bond acceptors, and hydrogen-bond donors/acceptor. Each type is represented as a sphere with a predefined radius and is assigned to a functional group in a molecule. After molecular superposition, the overlaps of the spheres are scored.

The program works as follows. First, a large molecule with its physicochemical properties represented by spheres is fixed at the center of a large box, and another smaller molecule, also with spheres representing its physicochemical properties, is translated and rotated in the box. The translational increment is 1 Å, and the center of mass is translated onto the body-centered-cubic lattice-points made in the circumscribed large-volume rectangular box. The rotation is performed on each of the lattice points. The ranges of the three Eulerian angles are $0° \leq \phi, \varphi < 360°$, and $0° \leq \theta \leq 180°$. The rotational increment is 4°. Second, at every translation or rotation, the property spheres that overlap are determined by calculating the distances between the spheres of the molecules. Third, overlaps of the spheres are scored so that points are added when atomic groups with the same physicochemical properties overlap, and points are subtracted when atomic groups with different physicochemical properties overlap, according to the scoring table (19). Atomic groups without overlaps are not scored.

These three operations are repeated to determine the orientation with the highest score and the smallest rms deviation (rmsd) of the distances of the overlapped atomic groups between the two molecules.

3D-QSAR Analyses: Determination of the Binding Conformation Using CoMFA

The SUPERPOSE program identified several plausible binding conformations. We therefore carried out comparative molecular field analysis (CoMFA) to determine the binding conformation of ligands to rat Mrp2 and to obtain 3D structure-activity relationships.

Table I. Results of Conformational Analysis by CAMDAS

	Number of conformers	ΔE (kcal/mol)	Number of conformers within 12 kcal/mol
Training set			
1	7777	15.570	3846
2	16	14.406	15
3	262	18.565	234
4	876	18.877	798
5	251	16.972	240
6	7777	13.951	5723
7	3121	1112.579	1576
8	479	54.432	316
9	264	32.593	180
10	2547	1013.488	2387
11	3957	978.039	3530
12	5937	53.872	1533
13	177	13.669	176
14	3078	52.334	2832
15	3069	1028.764	2915
16	5135	32.084	3856
Test set			
A	36	480.492	20
B	7777	86.823	4966

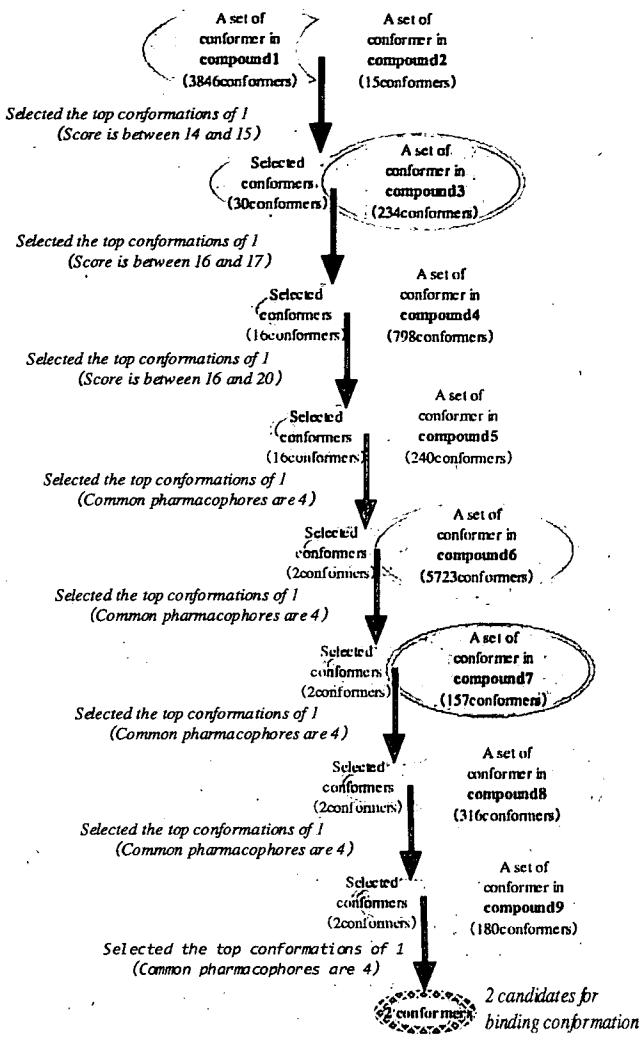

Fig. 3. Flowchart of SUPERPOSE.

The atomic charges of each conformer were calculated using the semiempirical molecular orbital program package MOPAC93 MNDO/ESP, in order to evaluate the electrostatic field in CoMFA. Conventional CoMFA was performed using the QSAR option of SYBYL (Tripos, Inc., St. Louis, MO, USA), with the Michaelis constant (K_m) (22) of each ligand included as bioactive data, as shown in Figs. 1 (training set) and 2 (test set). For the K_m-determination experiments, CMVs were prepared from male Sprague-Dawley (SD) rats, and the transport study was performed using the rapid-filtration technique, as described previously (11,12). All of the compounds were mainly excreted into the bile via rat Mrp2, as biliary excretion in EHBRs and/or the ATP-dependent uptake of each compound into CMVs prepared from EHBRs was disrupted. Therefore, the K_m values for the uptake into CMVs prepared from SD rats corresponded to those for rat Mrp2.

Two calculations were carried out, using an sp^3 carbon probe atom with a charge of +1 and either the steric and electrostatic components or the steric, electrostatic, and calculated log P (C log P) components. The calculated values of log P were estimated using the CLOGP program (Daylight, C.I.S. Inc., Rochester, NY, USA). The CoMFA QSAR equations were calculated with the partial least squares (PLS) algorithm. The optimal number of components in the final CoMFA PLS model was determined using the cross-validated R^2 (q^2) values obtained from the leave-one-out cross-validation technique. The CoMFA PLS model with the highest q^2 values was selected to estimate the binding conformation of ligands for rat Mrp2.

RESULTS

Sampling of a Set of Conformers of Each Ligand

Using the CAMDAS program, we carried out conformational analyses of ligand molecules bound to rat Mrp2. The high-temperature MD calculation was used with a potential function without an electrostatic interaction term and a hydrogen-bonding term to avoid undesirable intramolecular interactions (Figs. 1 and 2). The CAMDAS calculations gave many conformers of the 18 compounds, as shown in Table I. The sets of conformers of compounds **1–9**, the structures of which were significantly different from one another and showed relatively low K_m values, were used by the SUPERPOSE

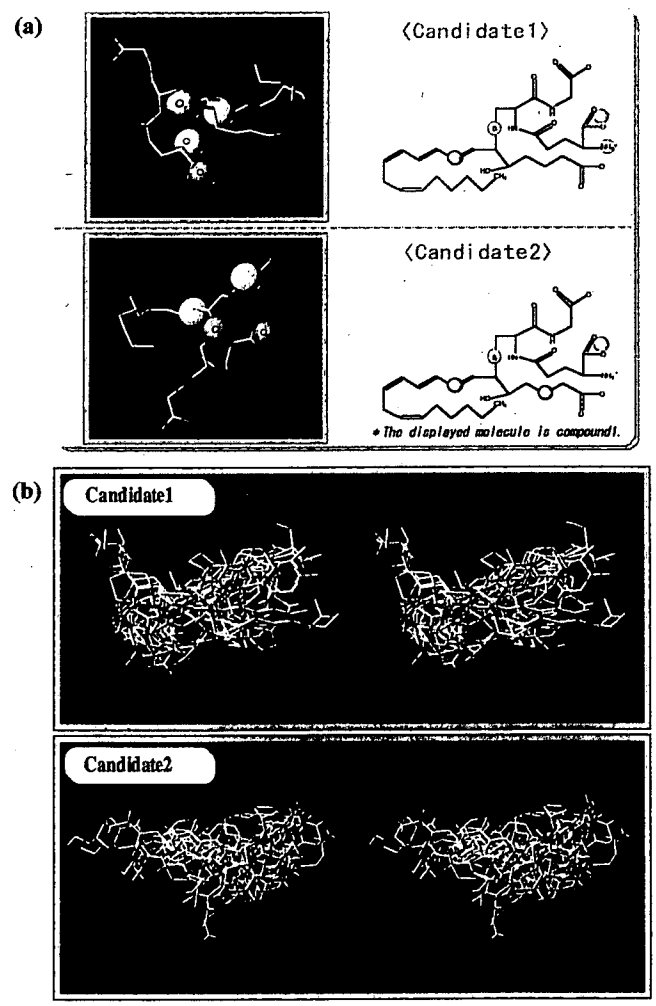

Fig. 4. (a) Property spheres common to compounds **1–9**. (b) Stereo views of superposed compounds in the training set (yellow molecule: compound **1**).

Table II. Results of CoMFA

Field type		Candidate 1		Candidate 2	
		ST + EL	ST + EL + C log P	ST + EL	ST + EL + C log P
Cross-validated	q^2	0.03	0.01	0.36	0.59
	s_{press}	1.21	1.15	0.80	0.64
No. of components		7	6	3	3
Conventional	r^2	1.00	1.00	0.99	0.99
	F	30122.14	2114.33	485.66	613.30
	s	0.01	0.03	0.09	0.08
Contribution (%)	ST	56.6	53.1	60.2	63.0
	EL	43.4	40.5	39.8	33.4
	C log P[a]	—	6.4	—	3.6

St, steric field; EL, electrostatic field; CoMFA, comparative molecular-field analysis.
[a] log P calculated by CLOGP.

program to determine the 3D pharmacophore of the ligand and to obtain the candidate binding conformations.

Selection of Candidate Binding Conformations

As shown in Table I, relatively stable conformers with molecular energies within 12 kcal/mol from the global minimum were selected as the conformers to be superposed. The cutoff value of 12 kcal/mol was confirmed in our previous study (19). For each ligand, the atomic groups that the property spheres were assigned to are shown in Figs. 1 (training set) and 2 (test set).

Initially, 3846 conformers of compound **1** and 15 conformers of compound **2** were superposed (Fig. 3). Each overlap was ranked on the basis of the SUPERPOSE score and the rmsd. As a result, we selected 30 conformers of compound **1** that represented good overlaps, with scores ranging between 14 and 15. Next, these 30 conformers of compound **1** and 234 conformers of compound **3** were superposed. As a result, we selected 16 conformers of compound **1** that showed good overlaps with conformers of compound **3**, with scores ranging between 16 and 17. The 16 selected conformers of compound **1** were then superposed to 798 conformers of compound **4**. No change was observed in the number of good overlaps at this stage, with scores ranging between 16 and 20 for all of the conformers. All 16 conformers of compound **1** were therefore superposed with 240 conformers of compound **5**. There were only two good overlaps for the superposition of compound **1** with compound **5**, with four commonly overlapped functional groups. Using the same method, the selected conformers of compound **1** were superposed to conformers of compounds **6–9** (Fig. 3). We finally obtained two conformers of compound **1** that were considered to be good candidates for the binding conformation. Figure 4a shows the common property spheres; namely, the pharmacophores obtained by superposition using compounds **1–9**.

Next, each candidate for the binding conformation was superposed to conformers of compounds **10–16** in the training set. The atomic groups that the ligand property spheres were assigned to are shown in Fig. 1. In this way, candidate binding conformations of compounds **10–16** were obtained. We then estimated the molecular alignment of ligand molecules (compounds **1–16**) that were essential to CoMFA (Fig. 4b). The

Table III. The Values of $\log(1/K_m)$ Calculated Using the Final CoMFA QSAR Model Compared with Experimental Data

	Experimental	Calculated	Residual
Compounds in the training set			
1 Leukotriene C4	6.60	6.70	−0.10
2 *p*-Nitrophenyl glucuronide	4.70	4.60	0.10
3 SN-38 glucuronide, lactone	5.64	5.63	0.01
4 SN-38 glucuronide, carboxylate	6.02	5.90	0.12
5 E3040 glucuronide	5.42	5.36	0.06
6 Leukotriene D4	5.82	5.77	0.05
7 *N*-acetyl leukotriene E4	5.28	5.33	−0.05
8 (*S*)-Grepafloxacin-glucuronide	5.00	5.00	0.00
9 (*R*)-Grepafloxacin-glucuronide	4.77	4.83	−0.06
10 L-Methotrexate	3.52	3.47	0.05
11 2,4-Dinitrophenyl-*S*-glutathione	4.68	4.76	−0.08
12 BQ-123	4.53	4.46	0.07
13 SN-38, carboxylate	4.16	4.25	−0.09
14 Temocaprilate	4.03	4.09	−0.06
15 5-Methyltetrahydrofolate	3.90	3.84	0.06
16 CPT-11, carboxylate	3.63	3.69	−0.06
Compounds in the test set			
A BQ-485	5.19	5.10	0.09
B MX-68	3.68	4.16	−0.48

two candidates of binding conformation of ligands for rat Mrp2 generated two types of molecular alignments, as shown in Fig. 4b. We also obtained binding conformation candidates for compounds **A–B** for the test set using a similar method to the training set. The test set was used to evaluate the predictive power of the CoMFA model obtained using the training set.

Determination of the Binding Conformation by CoMFA

CoMFA calculations were carried out using the two molecular alignments. The atomic charges of each conformer were calculated using MOPAC93 MNDO/ESP to evaluate the electrostatic field in CoMFA. Conventional CoMFA was performed with the QSAR option of SYBYL. For each molecular alignment (candidate 1 and candidate 2), two types of calculations were carried out together with an sp^3 carbon probe atom with a +1 charge: the first used steric and electrostatic fields, and the second used steric and electrostatic fields along with calculated values of log P (C log P). The CoMFA QSAR equations were calculated with the PLS algorithm. The optimal number of components in the final CoMFA PLS model was determined using the cross-validated R^2 (q^2) values obtained by the leave-one-out technique. The cross-validated R^2 (q^2) values, the standard error of the predictive sum of squares (s_{press}), and the standard error of the estimate (r^2) are listed in Table II for each candidate. The CoMFA PLS model with the highest q^2 values was assumed to best explain the binding conformation.

A good CoMFA model with three PLS components was obtained using the steric and electrostatic fields along with C log P for candidate 2. The final CoMFA model had a q^2 value of 0.59 with six PLS components, an s_{press} value of 0.64, an r^2 value of 0.99, and a standard error of 0.08. The experimental and calculated values of $\log(1/K_m)$ for each compound in the training set are listed in Table III. The property spheres shown in Fig. 5 illustrate the important atomic groups for the binding of each ligand molecule to rat Mrp2.

We also investigated the predictivity of the final CoMFA model using the test set of compounds. The values of $\log(1/K_m)$ calculated using the CoMFA model of candidate 2 with the steric field, electrostatic field, and C log P showed good agreement with the experimental values (Table III). We therefore concluded that the 3D structure of candidate 2 reflects the binding conformation of ligands for rat Mrp2. In the test set, the calculated value of $\log(1/K_m)$ for BQ-485 (5.10) compared well with the experimental value (5.19), whereas the calculated value of MX-68 contained a larger error (0.48). This might be the result of the difficulties of determining the atomic charges of MX-68, which has a pteridine ring, using MOPAC93 MNDO/ESP.

Figure 6a shows a contour map of the steric field from the final CoMFA model, together with the binding conformation of compound **1**: the green contours indicate areas in which bulky atomic groups are sterically favorable for the binding affinity, and the yellow contours indicate areas in which bulky groups are unfavorable for the binding affinity. Figure 6b shows a contour

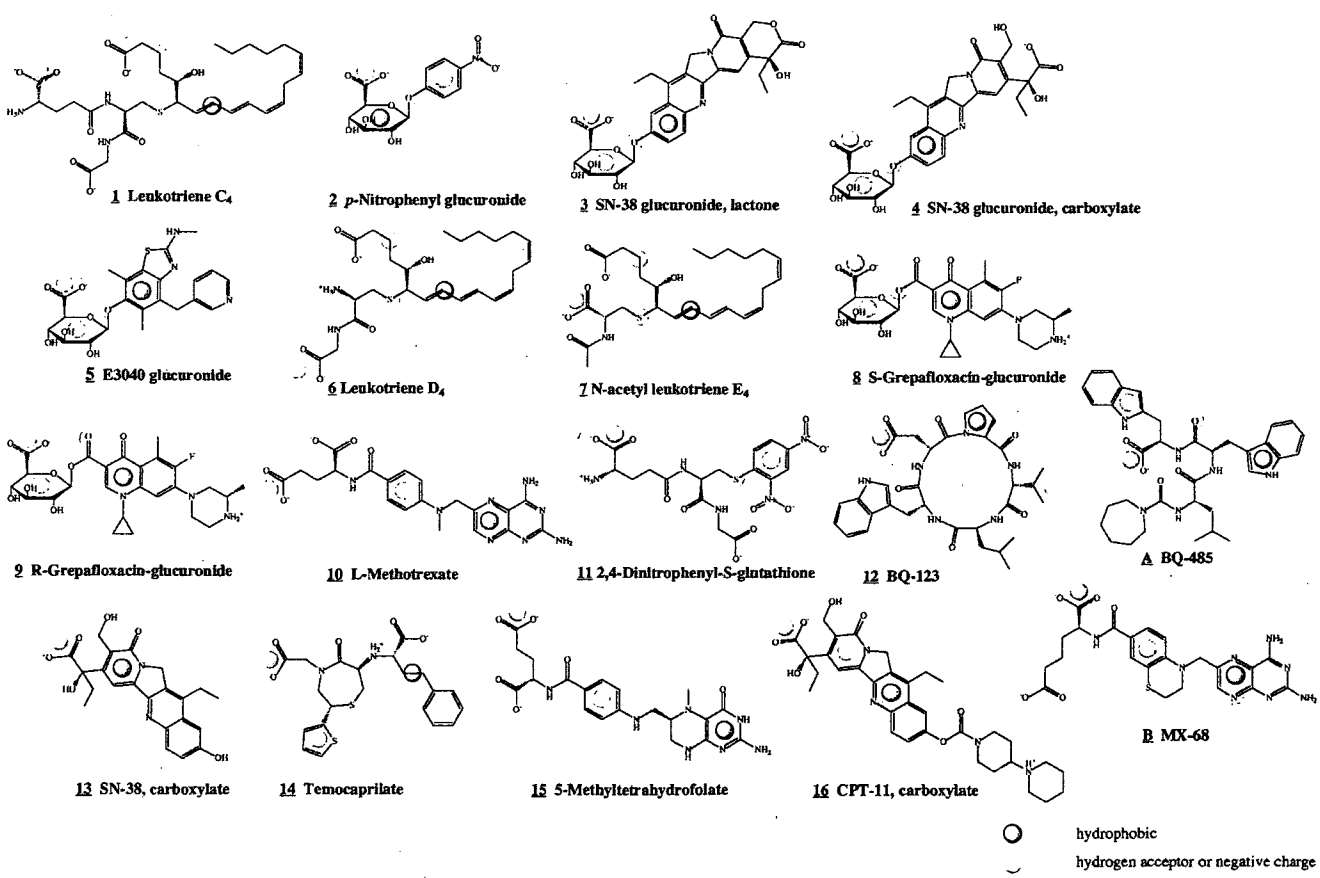

Fig. 5. Atomic groups involved in the binding of each ligand molecule to Mrp2/ABCC2.

(a) Steric field

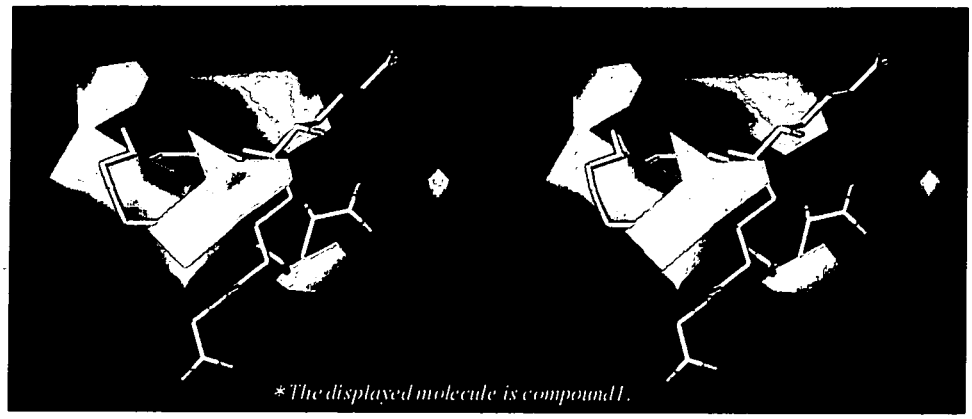

Green : Areas in which bulky atomic groups are sterically favorable for the binding affinity.

: Areas in which bulky groups are unfavorable for the binding affinity.

(b) Electrostatic field

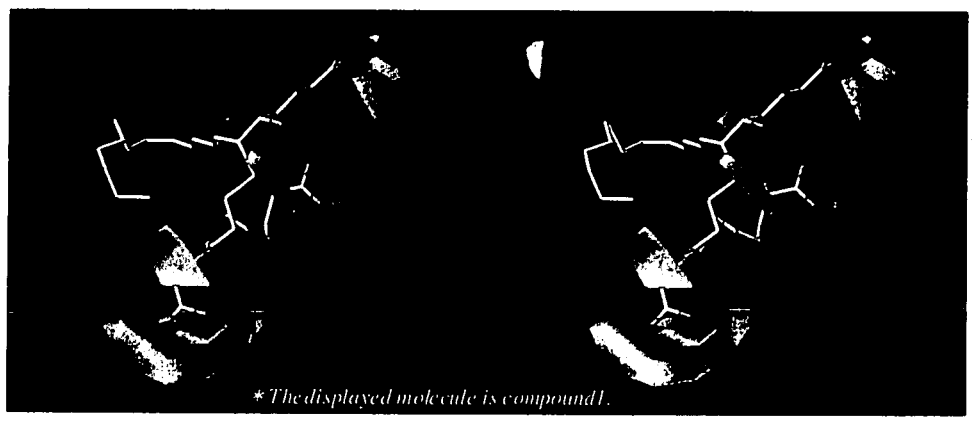

Blue : Areas in which atomic groups with positive charges are favorable for the binding affinity.

Red : Areas in which atomic groups with negative charges arefavorable for the binding affinity.

Fig. 6. Stereo views of contour maps obtained from the final CoMFA model. (a) Steric field. (b) Electrostatic field.

map of the electrostatic field from the final CoMFA model, together with the binding conformation of compound **1**: the blue contours indicate areas in which atomic groups with positive charges are advantageous to the binding of ligand with rat Mrp2, and the red contours show areas in which atomic groups with negative charges are favorable for the binding of ligand with rat Mrp2. The areas shown in the contour map are of great importance for explaining variation in the binding affinities of ligands with rat Mrp2.

DISCUSSION

Pharmacophore of Ligands for Rat Mrp2

We have identified a plausible binding conformation of ligands to rat Mrp2 by making full use of ligand-based drug design techniques. In this conformation, four property spheres that are common to all ligands were identified using the SUPERPOSE calculation. We propose that the spatial arrangement of the four functional groups expressed by these property spheres represents a 3D pharmacophore of ligands for rat Mrp2. Figure 7 shows a stereo view of these four property spheres along with the 3D structure of compound **1** and its structural formula. It appears that two hydrogen bond-acceptor groups (HA1 and HA2) and two hydrophobic groups (HP1 and HP2) are essential for the binding of ligands to rat Mrp2 and that these groups constitute the 3D pharmacophore. Figure 8 shows the relative distances between the four property spheres that represent the essential functional groups for ligand binding. The distances are as follows: HA1–HA2, ~5.0 &ARING;; HA1–HP1, ~5.3 &ARING;; HA1–

HP2, ~5.5 &ARING;; HA2–HP1, 4.7 &ARING;; HA2–HP2, 3.2 &ARING;; and HP1–HP2, 4.8 &ARING;.

Estimation of the Ligand-Binding Site of Rat Mrp2

A good CoMFA model was identified with the following parameters: a q^2 value of 0.59 with six PLS components, an s_{press} value of 0.64, an r^2 value of 0.99, and a standard error of 0.08. We suggest that the success of the CoMFA was a result of the use of the molecular alignment obtained using SUPERPOSE. This represents a unique and distinctive approach, in which the binding conformation and 3D pharmacophore of a ligand are estimated using ligand-based drug design techniques and are then applied to the molecular alignment, which is essential to CoMFA.

On the basis of the 3D pharmacophore and the contour map obtained from the CoMFA calculation, we have estimated the structure of the ligand-binding site of rat Mrp2 (Fig. 9). The four primary binding sites correspond to the 3D pharmacophore, comprising the four functional groups that are essential for the binding of ligands to rat Mrp2. The model also suggests that secondary binding sites, which correspond to specific contour levels in the CoMFA contour map, are important in explaining the variation of the binding affinities of ligands to rat Mrp2.

In conclusion, we propose that both hydrophobic and electrostatic interactions have vital roles in the binding of ligands to rat Mrp2. Ligand recognition seems to be achieved through interactions in the two hydrophobic sites and the two electrostatically positive sites (primary binding sites). Moreover, the broad substrate specificity of rat Mrp2 might be achieved by combinations of the secondary binding sites (two electrostatically positive sites and two electrostatically negative sites) with the primary binding sites.

The method described here for determining the binding conformation of ligands represents a powerful tool in cases where ligands have the same binding mode to the target protein. Of course, it should be noted that different binding modes might exist for some ligands; however, all of the ligands used in this analysis appeared to have the same binding mode, according to the results of the CoMFA. We believe that our data will be useful in the development of new com-

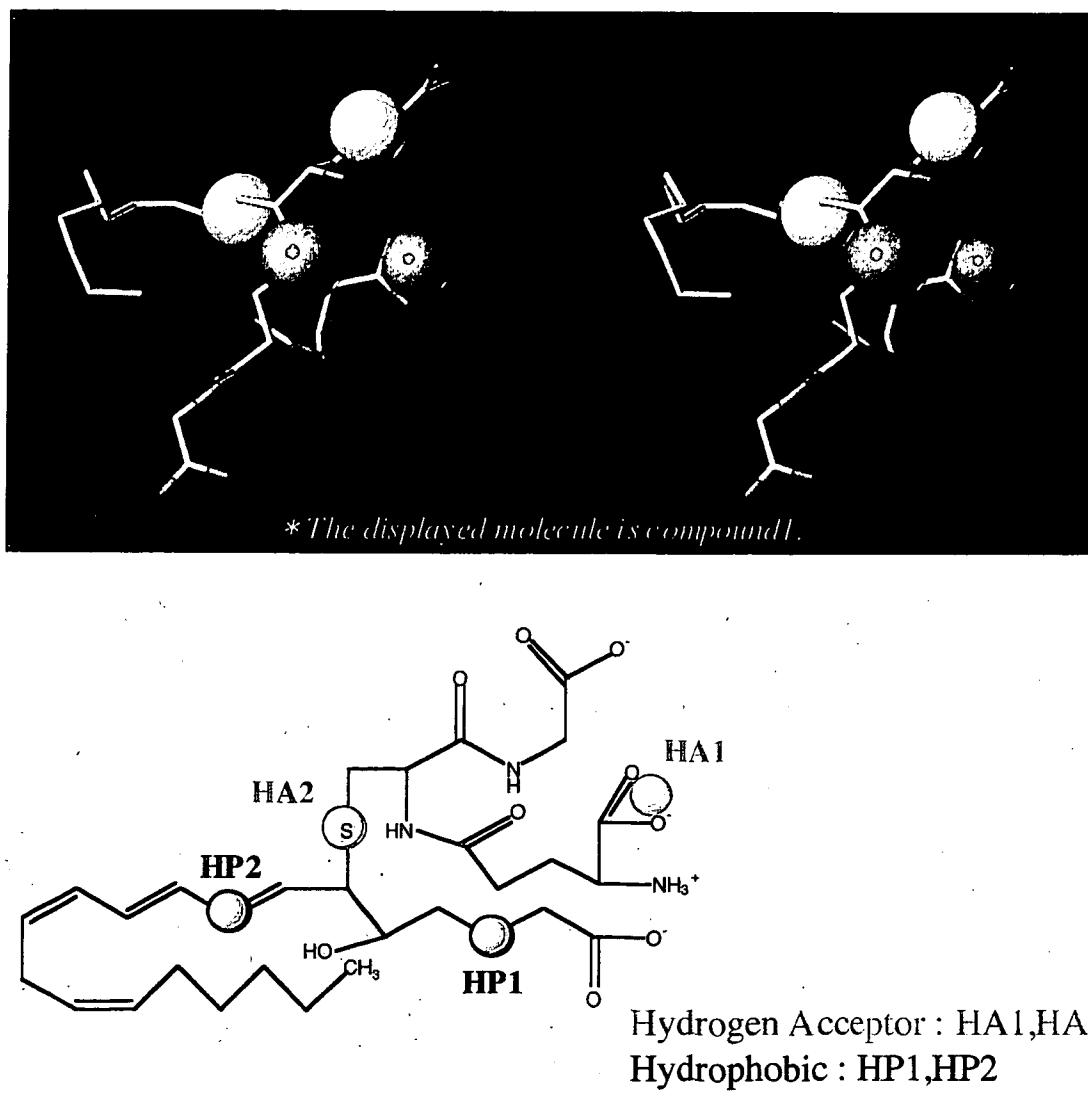

Fig. 7. A stereo view of the four property spheres that represent a 3D pharmacophore of ligands for Mrp2/ABCC2 and the 3D structure of compound **1** together with its structural formula.

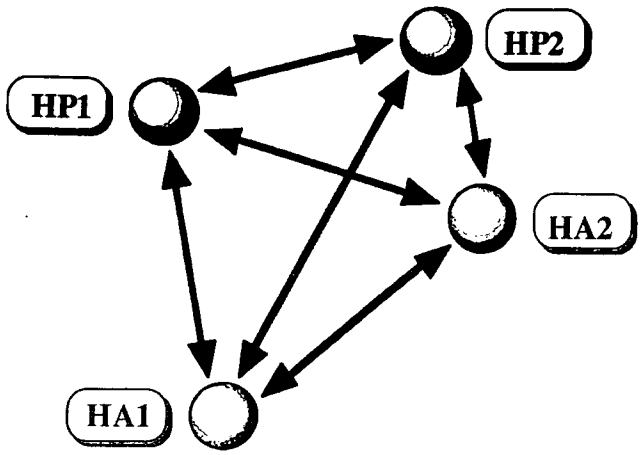

	Relative distances (Å)
HA1 - HA2	5.0 ± 0.9
HA1 - HP1	5.3 ± 0.7
HA1 - HP2	5.5 ± 1.6
HP1 - HA2	4.7 ± 0.8
HP1 - HP2	4.8 ± 1.1
HA2 - HP2	3.2 ± 1.2

Fig. 8. Relative distances between the four property spheres representing the functional groups that are essential for ligand binding.

compounds using the CoMFA QSAR model in order to evaluate their affinity for Mrp2.

REFERENCES

1. O. R. P. Elferink, D. K. Meijer, F. Kuipers, P. L. Jansen, A. K. Groen, and G. M. Groothuis. Hepatobiliary secretion of organic compounds; molecular mechanisms of membrane transport. *Biochim. Biophys. Acta* **1241**:215–268 (1995).
2. M. Yamazaki, H. Suzuki, and Y. Sugiyama. Recent advances in carrier-mediated hepatic uptake and biliary excretion of xenobiotics. *Pharm. Res.* **13**:497–513 (1996).
3. D. Keppler and J. Konig. Hepatic canalicular membrane 5: expression and localization of the conjugate export pump encoded by the *Mrp2* (*cMRP/cMOAT*) gene in liver. *FASEB J.* **11**:509–516 (1997).
4. K. Ito, H. Suzuki, T. Hirohashi, K. Kume, T. Shimizu, and Y. Sugiyama. Molecular cloning of canalicular multispecific organic anion transporter defective in EHBR. *Am. J. Physiol.* **272**:G16–G22 (1997).
5. C. C. Paulusma, P. J. Bosma, G. J. Zaman, C. T. Bakker, M. Otter, G. L. Scheffer, R. J. Scheper, P. Borst, and O. R. P. Elferink. Congenital jaundice in rats with a mutation in a multidrug resistance-associated protein gene. *Science* **271**:1126–1128 (1996).
6. K. Sathirakul, H. Suzuki, K. Yasuda, M. Hanano, O. Tagaya, T. Horie, and Y. Sugiyama. Kinetic analysis of hepatobiliary transport of organic anions in Eisai hyperbilirubinemic mutant rats. *J. Pharmacol. Exp. Ther.* **265**:1301–1312 (1993).
7. K. Sathirakul, H. Suzuki, T. Yamada, M. Hanano, and Y. Sugiyama. Multiple transport systems for organic anions across the bile canalicular membrane. *J. Pharmacol. Exp. Ther.* **268**:65–73 (1994).
8. M. Yamazaki, S. Akiyama, K. Ni'inuma, R. Nishigaki, and Y. Sugiyama. Biliary excretion of pravastatin in rats: contribution of the excretion pathway mediated by canalicular multispecific organic anion transporter. *Drug Metab. Dispos.* **25**:1123–1129 (1997).
9. H. Ishizuka, K. Konno, H. Naganuma, K. Sasahara, Y. Kawahara, K. Niinuma, H. Suzuki, and Y. Sugiyama. Temocaprilat, a novel angiotensin-converting enzyme inhibitor, is excreted in bile via an ATP-dependent active transporter (cMOAT) that is deficient in

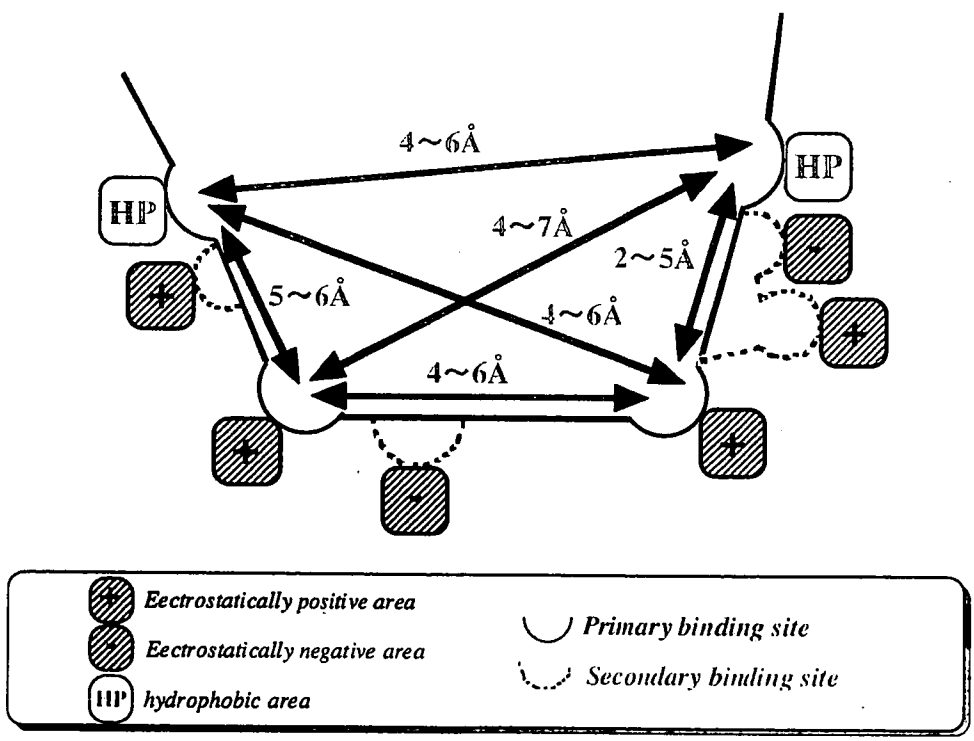

Fig. 9. Ligand-binding region of Mrp2/ABCC2 estimated using the 3D pharmacophore and CoMFA contour map.

Eisai hyperbilirubinemic mutant rats (EHBR). *J. Pharmacol. Exp. Ther.* **280**:1304–1311 (1997).
10. H. C. Shin, Y. Kato, T. Yamada, K. Niinuma, A. Hisaka, and Y. Sugiyama. Hepatobiliary transport mechanism for the cyclopentapeptide endothelin antagonist BQ-123. *Am. J. Physiol.* **272**: G979–G986 (1997).
11. T. Ishikawa, M. Muller, C. Klunemann, T. Schaub, and D. Keppler. ATP-dependent primary active transport of cysteinyl leukotrienes across liver canalicular membrane. Role of the ATP-dependent transport system for glutathione S-conjugates. *J. Biol. Chem.* **265**:19279–19286 (1990).
12. K. Kobayashi, Y. Sogame, H. Hara, and K. Hayashi. Mechanism of glutathione S-conjugate transport in canalicular and basolateral rat liver plasma membranes. *J. Biol. Chem.* **265**:7737–7741 (1990).
13. T. Nishida, Z. Gatmaitan, J. Roy-Chowdhry, and I. M. Arias. Two distinct mechanisms for bilirubin glucuronide transport by rat bile canalicular membrane vesicles. Demonstration of defective ATP-dependent transport in rats (TR-) with inherited conjugated hyperbilirubinemia. *J. Clin. Invest.* **90**:2130–2135 (1992).
14. O. Takenaka, T. Horie, K. Kobayashi, H. Suzuki, and Y. Sugiyama. Kinetic analysis of hepatobiliary transport for conjugated metabolites in the perfused liver of mutant rats (EHBR) with hereditary conjugated hyperbilirubinemia. *Pharm. Res.* **12**:1746–1755 (1995).
15. M. Trauner, M. Arrese, C. J. Soroka, M. Ananthanarayanan, T. A. Koeppel, S. F. Schlosser, F. J. Suchy, D. Keppler, and J. L. Boyer. The rat canalicular conjugate export pump (Mrp2) is down-regulated in intrahepatic and obstructive cholestasis. *Gastroenterology* **113**:255–264 (1997).
16. X. Y. Chu, Y. Kato, and Y. Sugiyama. Multiplicity of biliary excretion mechanisms for irinotecan, CPT-11, and its metabolites in rats. *Cancer Res.* **57**:1934–1938 (1997).
17. H. Suzuki and Y. Sugiyama. Role of transporters in the detoxification of xenobiotics: recent advances in the study of cMOAT/MRP. *Tanpakushitsu Kakusan Koso* **42**:1273–1284 (1997).
18. H. Tsujishita and S. Hirono. CAMDAS: an automated conformational analysis system using molecular dynamics. *J. Comput. Aided Mol. Des.* **11**:305–315 (1997).
19. K. Iwase and S. Hirono. Estimation of active conformations of drugs by a new molecular superposing procedure. *J. Comput. Aided Mol. Des.* **13**:499–512 (1999).
20. R. D. Cramer, D. E. Patterson, and J. D. Bunce. Comparative molecular field analysis (CoMFA). 1. Effect of shape on binding of steroids to carrier proteins. *J. Am. Chem. Soc.* **110**:5959–5967 (1988).
21. N. L. Allinger. Conformational analysis. 130. MM2. A hydrocarbon force field utilizing V1 and V2 torsional terms. *J. Am. Chem. Soc.* **99**:8127–8134 (1977).
22. H. Suzuki and Y. Sugiyama. Transporters for bile acids and organic anions. *Pharm. Biotechnol.* **12**:387–439 (1999).

Pharmaceutical Research, Vol. 22, No. 4, April 2005 (© 2005)
DOI: 10.1007/s11095-005-2502-1

Research Paper

Treatment of Hyperbilirubinemia in Eisai Hyperbilirubinemic Rat by Transfecting Human MRP2/ABCC2 Gene

Masakazu Hirouchi,[1] Hiroshi Suzuki,[1] and Yuichi Sugiyama[1,2]

Received October 8, 2004; accepted January 10, 2005

Purpose. Multidrug resistance–associated protein 2 (MRP2/ABCC2) is predominantly expressed in the liver canalicular membrane and plays an important role in the biliary excretion of organic anions including glucuronide and glutathione conjugates. The purpose of this study is to construct a new evaluation system for human MRP2 by expressing human MRP2 in Eisai hyperbilirubinemic rat (EHBR) liver, the rat Mrp2 function of which is hereditarily defective.
Methods. In order to express human MRP2 in liver, we used the Tet-off adenovirus expression system. After 72 h infection, we evaluated the protein expression and localization in the liver and the transport activity of [^{3}H]$E_2$17ßG and [^{3}H]DNP-SG by preparing canalicular membrane vesicles (CMVs). We also evaluated the biliary excretion and plasma concentration of DBSP after bolus administration and the plasma concentration of endogenous direct and indirect bilirubin.
Results. The localization of human MRP2 in EHBR liver was found to be at the bile canalicular membrane. Clear ATP-dependent uptake of [^{3}H]$E_2$17ßG and [^{3}H]DNP-SG into CMVs was observed by using the CMVs prepared from the liver where human MRP2 was transfected. Furthermore, the blood to bile clearance of DBSP increased approximately 3-fold after expression of human MRP2. In addition, the plasma direct bilirubin level in EHBR was reduced by the expression of human MRP2.
Conclusion. These results suggest that this evaluation system for human MRP2 may be useful for evaluating the function of human MRP2.

KEY WORDS: biliary excretion; EHBR; liver; MRP2.

INTRODUCTION

Multidrug resistance–associated protein 2 (MRP2/ABCC2) is a glycosylated integral plasma membrane protein belonging to the ATP-binding cassette transporter family. Its function has been studied extensively by comparing the transport across the bile canalicular membrane between normal and Mrp2-deficient mutant rats such as Eisai hyperbilirubinemic rats (EHBRs). Now, it is established that Mrp2 is mainly located on the bile canalicular membrane and the apical membrane of enterocytes and plays a primary role in biliary excretion and in restricting the oral absorption of its substrates, including anionic drugs and glutathione and glucuronide conjugates of xenobiotics (1–7). It has also been established that mutations in the MRP2 gene are responsible for the pathogenesis of Dubin-Johnson syndrome (DJS), characterized by a defect in the biliary excretion of bilirubin glucuronides (7–9). We have recently focused on the SNPs variants/mutants of MRP2, because, due to the fact that some MRP2 mutations found in DJS patients are associated with a loss of transport activity and/or the ability to traffick to the apical membrane by the single amino acid alteration (10,11), it is possible that the MRP2 SNPs may also be associated with alterations in function and, consequently, may be responsible for the inter-individual differences in the disposition of substrate drugs. Previously, we have characterized the function of SNPs variants/mutants of MRP2 using LLC-PK1 cells (12). Although the wild-type MRP2 was exclusively localized at the apical membrane, S789F and A1450T MRP2 were located not only at the apical membrane but also in the intracellular compartment, suggesting that the *in vivo* function of these two kinds of variants may be lower than wild type MRP2 (12).

However, there are some reports which suggest that the localization of some membrane proteins in cultured cells does not necessarily reflect the localization in tissues. For example, rat Oat-K1 is localized at the apical membrane in the proximal tubules (13), whereas this transporter localizes at the basolateral membrane in LLC-PK1 cells, derived from porcine kidney (14). Moreover, rat serotonin transporter and norepinephrine transporter are known to be sorted to the apical compartment (axolemmal domain) of neuronal cells, whereas these transporters are sorted to the basolateral membrane in MDCK cells, derived from canine kidney (15). One

[1] School of Pharmaceutical Sciences, University of Tokyo, Hongo, Bunkyo-ku, Tokyo 113-0033, Japan.
[2] To whom correspondence should be addressed. (e-mail: sugiyama@mol.f.u-tokyo.ac.jp)

ABBREVIATIONS: Ad, adenovirus; CMV, canalicular membrane vesicle; DBSP, dibromosulfophtalein; DJS, Dubin-Johnson syndrome; DNP-SG, 2,4-dinitrophenyl-*S* glutathione; $E_2$17ßG, 17β-estradiol 17β-D-glucuronide; EHBR, Eisai hyperbilirubinemic rats; MRP, multidrug resistance–associated protein; pfu, plaque-forming unit; SNPs, single nucleotide polymorphisms; TRE, tet-responsive element; tTA, tetracycline-responsive transcriptional activator.

of the hypotheses for these alterations of the cellular localization is that some proteins which are necessary for the apical targeting under physiologic conditions are deficient in cultured cells. Concerning this point, it is essential to determine the localization of SNPs variants/mutants of MRP2 in human liver, although such determination is quite difficult. Therefore, we have planned to construct an *in vitro* evaluation system which may reflect the cellular localization under physiologic conditions. Thus, we have focused on using the Eisai hyperbilirubinemic rat (EHBR), as the mutation in the Mrp2 gene leads to the absence of Mrp2 protein in this mutant strain (16,17).

The purpose of this study is to establish a new system for evaluating the function of human MRP2 by expressing this transporter on the canalicular membrane of EHBR liver. To express human MRP2 in EHBR liver, we used Tet-off recombinant adenovirus systems. The expression level, localization and the transport function of human MRP2 in EHBR liver were analyzed.

MATERIALS AND METHODS

Materials

[^{3}H]$E_2$17ßG (51.0 μCi/nmol) with a purity of 98.5% was purchased from New England Nuclear (Boston, MA, USA). Unlabeled and [^{3}H]labeled 2,4-dinitrophenyl-*S*-glutathione ([^{3}H]DNP-SG, 44.8 μCi/nmol) were synthesized as described previously (18). ATP, creatine phosphate, creatine phosphokinase, acivicin, and glutathione *S*-transferase were purchased from Sigma Chemical (St. Louis, MO, USA). All other chemicals used were commercially available and of reagent grade. Sprague-Dawley rats (normal rats) and EHBR weighing approximately 180 g were used throughout the experiments.

Construction of Recombinant Adenoviruses Containing MRP2

Human MRP2 cDNA located between the Not I and Nco I sites of pBluescript SK(-) (Stratagene, La Jolla, CA, USA) was provided by Dr. Kuwano (Kyushu University School of Medicine). The MRP2 cDNA was subcloned into the Not I and Nco I sites of the pTRE shuttle, resulting in the production of pTRE shuttle-MRP2. pTRE shuttle-MRP2 has I-CeuI and PI-SceI sites upstream and downstream of the MRP2 expression cassette, respectively. The I-CeuI / PI-SceI digested fragments of pTRE shuttle-MRP2 were ligated with I-CeuI / PI-SceI digested Adeno-X Viral DNA (BD Biosciences, Palo Alto, CA, USA), resulting in pAd-MRP2. pAd containing tetracycline-responsive transcriptional activator (tTA) (pAd-tTA) was purchased from Clontech (Palo Alto, CA, USA).

To generate the recombinant viruses, both pAd-MRP2 and pAd-tTA were digested with PacI. Linearized DNAs were transfected to HEK293 cells grown on a 12-well dish with Fugene 6 (Roche Diagnostics Corp., Tokyo, Japan) according to the manufacturer's instructions. Viruses (Ad-MRP2 and Ad-tTA) were prepared as described previously (19). Recombinant viruses were purified by CsCl gradient centrifugation, dialyzed with a solution containing 10 mM Tris (pH 7.5), 1 mM $MgCl_2$, and 10% glycerol, and stored in aliquots at −80°C. Then, the resulting virus titer was determined as described previously (20).

Infection of Recombinant Adenovirus and the Preparation of Canalicular Membrane Vesicles

The adenoviruses were injected to EHBR via the tail vein. EHBR were infected with both Ad-MRP2 and Ad-tTA to express human MRP2 (MRP2-EHBR). For the negative control, EHBR were infected only with Ad-tTA (control EHBR). CMVs were prepared from EHBR liver 72 h after adenovirus infection as described previously (18) and kept as a suspension in 50 mM Tris buffer (pH 7.4) containing 250 mM sucrose. The membrane vesicles were frozen in liquid N_2 and stored at −80°C until required. The activity of the CMVs was checked by measuring the ATP-dependent uptake of standard substrates, [^{3}H]$E_2$17ßG (400 nM) and [^{3}H]DNP-SG (1 μM) for a 5-min incubation at 37°C. Protein concentrations were determined by the Lowry method.

Immunoblots

For the Western blot analysis, CMVs were dissolved in 3x SDS sample buffer (New England BioLabs, Beverly, MA, USA) and subjected to electrophoresis on a 7% SDS-polyacrylamide gel with a 4.4% stacking gel. The molecular weight was determined using a prestained protein marker (New England BioLabs). Proteins were transferred electrophoretically to a nitrocellulose membrane (Millipore, Bedford, MA, USA) using a blotter (Bio-Rad Laboratories, Richmond, CA, USA) at 15 V for 1 h The membrane was blocked with 2.5% skimmed milk for 1 h at room temperature. Then, the membrane was incubated for 40 min at room temperature with anti-MRP2 rabbit serum, diluted with skimmed milk (1:500), which was raised against 12 amino acids at the carboxyl terminus of the deduced MRP2 sequence (EAGIENVNSTKF). For the detection of MRP2, the membrane was allowed to bind to Alexa Fluor 680 goat anti-rabbit IgG (H+L) (Molecular Probes, Inc., Eugene, OR, USA). The fluorescence was assessed in a densitometer (Odyssey, ALOKA, Tokyo, Japan).

Immunofluorescence

For the immunofluorescence, liver from MRP2-EHBR and control-EHBR was removed 72 h after infection. Cryostat sections (5 μm in thickness) were fixed in methanol at −20°C for 10 min, washed three times with PBS, and blocked with 1% BSA/PBS at room temperature for 15 min. Then, slices were incubated with the monoclonal antibody against MRP2 (M2-6 (Molecular Probes Inc., Eugene, OR, USA), diluted 40-fold in PBS) for 1 h at room temperature. Following this, slices were washed three times with PBS and incubated with goat anti-mouse IgG Alexa 488 (Molecular Probes, Inc.) diluted 250-fold in PBS for 1 h at room temperature, and mounted in VECTASHIELD Mounting Medium (Vector Laboratories, Burlingame, CA, USA). The localization of the MRP2 protein was visualized by confocal laser microscopy (Zeiss LSM-510; Carl Zeiss Inc., Thornwood, NY, USA).

Vesicle Transport Assays

The uptake study of [^{3}H]$E_2$17βG (400 nM) and [^{3}H]DNP-SG (1 μM) was performed as reported previously (21). Briefly, the transport medium (10 mM Tris, 250 mM sucrose and 10 mM $MgCl_2 \cdot 6H_2O$, pH 7.4) contained the ligands, 5 mM ATP, and an ATP-regenerating system (10 mM creatine phosphate and 100 μg/ml of creatine phosphokinase). An aliquot of transport medium (17–18 μl) was mixed rapidly with the vesicle suspension (5 μg protein in 2–3 μl). The transport reaction was stopped by the addition of 1 ml ice-cold buffer containing 250 mM sucrose, 0.1 M NaCl and 10 mM Tris-HCl (pH 7.4). The stopped reaction mixture was filtered through 0.45-μm HA filters (Millipore Corp.) and then washed twice with 5 ml of the stop solution. The radioactivity retained on the filter was measured in a liquid scintillation counter (LS 6000SE, Beckman Instruments, Fullerton, CA, USA) after the addition of scintillation cocktail (Clear-sol I, Nacarai Tesque, Tokyo, Japan). Ligand uptake was normalized in terms of the amount of membrane protein.

Blood and Bile Sampling

Sprague-Dawley rats (normal rats) and EHBR were kept under ether anesthesia and then the femoral artery and vein were cannulated with polyethylene tubing (PE-50) for ligand administration and blood sampling, respectively. The common bile duct was also cannulated with PE-10. DBSP (10 μmol/kg) in saline was administered intravenously through the femoral vein cannula. Blood samples were obtained at given times. The rectal temperature was maintained at 37°C ± 0.5°C with a heat lamp.

Analysis of Specimens Obtained from *in Vivo* Experiments

To determine the DBSP concentrations, plasma and bile specimens were diluted with 50 mM Tris-HCl buffer (pH 7.4) free from bovine serum albumin, and then made alkaline by the addition of NaOH. Concentrations of DBSP in the diluted specimens were determined in a dual-wave length spectrophotometer (Hitachi Ltd., Tokyo, Japan) at a wavelength of 575 nm/620 nm. Direct and indirect bilirubin concentrations of some specimens were also determined using a test kit (Bilirubin BII-Test Wako, Wako Pure Chemical Industries, Ltd., Tokyo, Japan). Bile volume was measured gravimetrically, assuming a density of 1.0 for bile specimens.

RESULTS

Expression Level of MRP2 Protein in EHBR Liver

To determine the appropriate amount of adenoviruses for the protein expression of human MRP2 in EHBR liver, 1×10^9, 7.5×10^9, 1×10^{10}, and 2.5×10^{10} plaque-forming units (pfu) of both Ad-MRP2 and Ad-tTA were injected to EHBR through the tail vein. Presumably due to the liver toxicity of the viruses, EHBR infected with 1×10^{10} and 2.5×10^{10} pfu died soon after injection. The expression level of human MRP2 in the canalicular membrane fraction isolated from EHBR liver was examined by Western blot analysis. It was found that the human MRP2 antibody recognized the band with an approximate molecular weight of 190 kDa (Fig. 1), which is consistent with a previous report (22). When infected

Fig. 1. Expression of human MRP2 in CMVs. Expression of the human MRP2 protein was determined in CMVs (5 μg) isolated from control-EHBR and MRP2-EHBR by Western blot analysis.

with 7.5×10^9 pfu, the band density of MRP2 was approximately 5-fold higher compared with that in EHBR infected with 1×10^9 pfu (Fig. 1).

Localization of Human MRP2 in EHBR Liver

The localization of human MRP2 in EHBR liver was determined by immunofluorescence. Using an antibody against MRP2, the fluorescence signal was detected exclusively at the bile canalicular membrane of EHBR liver after simultaneous infection of Ad-tTA and Ad-MRP2 (Fig. 2). No

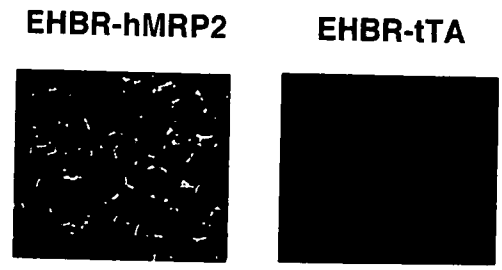

Fig. 2. Localization of human MRP2 in EHBR liver. The immunolocalization of MRP2 molecules in MRP2-EHBR was determined using a monoclonal antibody for human MRP2 (green). Nuclei were stained with PI (red).